Linear and Nonlinear Theory of Eigenfunction Scars

L. Kaplan*
Department of Physics and Society of Fellows,
Harvard University, Cambridge, MA 02138

E. J. Heller†
Department of Physics and Harvard-Smithsonian Center for
Astrophysics, Harvard University, Cambridge, MA 02138

The theory of scarring of eigenfunctions of classically chaotic systems by short periodic orbits is extended in several ways. The influence of short-time linear recurrences on correlations and fluctuations at long times is emphasized. We include the contribution to scarring of nonlinear recurrences associated with homoclinic orbits, and treat the different scenarios of random and nonrandom long-time recurrences. The importance of the local classical structure around the periodic orbit is emphasized, and it is shown for an optimal choice of test basis in phase space, scars must persist in the semiclassical limit. The crucial role of symmetry is also discussed, which together with the nonlinear recurrences gives a much improved account of the actual strength of scars for given classical orbits and in individual wavefunctions. Quantitative measures of scarring are provided and comparisons are made with numerical data.

I. INTRODUCTION

Some years ago Berry [1] suggested that quantum eigenstates of classically chaotic systems should locally look like random superpositions of plane waves of the same (local) wavevector magnitude k, producing Gaussian random fluctuations in position space. This is the natural quantum manifestation of complete classical uniformity on the energy hypersurface for chaotic systems. It is also a consequence of random matrix theory (RMT), assuming that this theory applies to classically chaotic systems [2]. On the other hand, Gutzwiller periodic orbit theory of the energy spectra of classically chaotic systems has enjoyed much success, and it would be strange if periodic orbits had no visible manifestation in the eigenstates. Indeed, exact solutions of the Schrödinger equation for classically chaotic systems sometimes exhibit obvious and apparently nonrandom patterns of concentration on periodic orbits. Other non-coordinate space representations such as projections onto coherent states (Husimi phase space) naturally show the same effect. This is a fully quantum phenomenon, although the explanation of scarring in terms of classical periodic orbits and their stability exponents [3] is based on semiclassical arguments. It is known that the structure of individual quantum eigenstates can often be well reproduced in the semiclassical approximation, ignoring "hard quantum" effects such as tunneling and diffraction [4]. Scars are surprising because classically (in the absence of phase coherence) there is no such accumulation of density near a periodic orbit in the long time limit for a bounded chaotic system. Scars are interesting because they stand out against the monotonous backdrop of wavefunction randomness over most of phase space. It has been shown that explicitly constructed "random" wavefunctions (random superpositions of plane waves with constant wavevector magnitude) show a ridge pattern that can be thought of as a precursor of true scarring [5].

Scars have now been seen in many studies, including experimental work in microwave cavities [6,7], tunnel junctions [8], and the hydrogen atom in a uniform magnetic field [9,10].

To the casual observer the scarring phenomenon finds its proof in visual evidence (*e.g.* heavily scarred wavefunctions when plotted in coordinate space). However there are quantitative reasons for scarring; the first theory for them [3] was based on wavepacket motion (in the semiclassical limit) along a periodic orbit, and used the *linearized* short time dynamics near the orbit. This was a Husimi phase space theory; subsequent work by Bogomolny [11] and Berry [12] were coordinate space and Wigner phase space theories, respectively. These also were based purely on the linearized dynamics in the vicinity of an unstable periodic orbit. Ref. [3] showed that scar strength for the heavily scarred states, as measured by the ratio of actual density to statistically expected density, was expected to be a function of the Lyapunov exponent λ only, tending to c/λ for small λ, where c is a constant. (Note the independence of $\hbar$.) That paper also remarked that scars are sometimes much stronger than this. At the other extreme, Steiner's work with systems of constant negative curvature was claimed to show no scarring when it was supposed to exist [13]. These

*kaplan@physics.harvard.edu
†heller@physics.harvard.edu

factors plus confusion over the definition and measures of scar strength have understandably caused much discussion of whether there is indeed a theory of scar strength. The work by Fishman, Agam, and co-workers [14–16] has provided additional perspectives, and a proposed measure for scars, about which we comment later.

The main points of this paper are (1) to point out that very often the original linear theory, together with a proper account of gaussian fluctuations and symmetry is sufficient to understand scar strength; (2) to show that scarring stronger than this may sometimes be understood in terms of identifiable *nonlinear* homoclinic recurrences associated with a given periodic orbit, the effect of which recurrences will turn out to be $\hbar$-dependent; (3) to firm up the existing definitions and measures of scarring; and (4) to extend the notion of scarring to classical structures associated with periodic orbits, as suggested already by the work of Voros [17]. We do not attempt here to treat the case of many periodic orbits of similar stability, period, and action contributing within one $\hbar$ cell in phase space. This can also dramatically enhance scarring, but it is a non-asymptotic effect which disappears in the $\hbar \to 0$ limit.

In the following section, we hope to clarify the concept of scarring. Then we provide a review of the original linear theory, for completeness and to establish the important concept of the spectral envelope, which we use heavily. After presenting the properties of scars as a localization phenomenon, we turn to considerations of discrete symmetries, and of nonlinear fluctuations about the envelope, which together explain many cases of enhanced wavefunction scarring. Connections with semiclassical theory are made here, and emphasis is placed on the constraints which the short-time dynamics places on the stationary properties of the system. Various measures of scarring are described, including ones which explicitly incorporate the linearized dynamics around a classical orbit. This is followed by numerical studies which show the expected amount of scarring according to the linear theory supplemented by gaussian random fluctuations, in the first statistical study of a large number of scarred states. Numerical evidence is also presented for the effects on scarring of individual homoclinic orbits, in a situation where the long-time recurrences are not random. We end with a discussion of the state of the theory of wavefunction scarring.

II. WHAT IS A SCAR?

We begin with a list of things which are *not* properties of scars, followed by a list of properties which are in fact associated with scars. Several of these statements will gradually become clearer in the theory sections to follow.

What scars are *not*:

- Scarring is not associated with stable classical orbits. These do of course attract wavefunction density strongly in some eigenstates, but the reasons are well understood in terms of the semiclassical theory of integrable systems [18]. The scarring phenomenon is also qualitatively distinct from the "bouncing ball" states associated with marginally stable orbits [19].

- Weak scars are not always visible to the "naked eye"; there is scarring nonetheless according to the definition given below. The amount of scarring associated with specific eigenstates varies significantly from state to state, though in accordance with a theoretically predicted distribution. Also orbits with larger instability exponents exhibit less scarring on average, and a statistical analysis may be necessary in such cases to determine that scarring is indeed present.

- Scarring is not a threat to ergodicity of wavefunctions in the sense of Schnirelman, Zelditch, and Colin de Verdiere [20], because the phase space area affected by scarring vanishes in the semiclassical limit, forming a narrower and narrower region around the periodic orbit.

- Scars are not merely associated with a one dimensional line along a periodic orbit; rather, they are associated also with the stable and unstable manifolds of that orbit. For this reason, a phase space study of scarring may often be more illuminating than a coordinate space projection.

- Scars do not disappear as $\hbar \to 0$, except in the sense that the total amount of scarring is expected to become distributed over an ever increasing number of eigenstates in that limit, while the region of phase space in which the eigenstates are scarred is simultaneously decreasing.

What scars are:

We begin with a definition, close to what was already given in the 1989 Les Houches proceedings [21]:

- *Definition:* A quantum eigenstate of a classically chaotic system has a *scar* of a periodic orbit if its density on the classical invariant manifolds near the periodic orbit is enhanced over the statistically expected density.

- Alternatively, an unstable periodic orbit is scarred when some eigenstates of the system have greater amplitude, and others less amplitude, along the orbit than would be predicted based on gaussian random fluctuations. Also, a wavepacket launched on or near such an orbit will have a tendency to return to the orbit, having larger overlaps with itself at long times than a wavepacket launched elsewhere in phase space.

- Scars can appear as strong enhancements in the eigenfunction coordinate space density surrounding periodic orbits, especially near self-conjugate points along the classical orbit, as shown by Bogomolny [11].

- Scar strength S, as measured by the projection of scarred eigenstates onto a coherent state centered on the scarring periodic orbit and aligned along the stable and unstable manifolds, is generically a function only of λ, the Lyapunov exponent for one period of the periodic orbit, and is $\hbar$-independent. For small λ, $S \to C/\lambda$, where C is a constant obtained by considering the linear theory at short times combined with random long-time fluctuations.

- Enhancements of the scarring phenomenon can occur in the presence of strong, isolated long-time recurrences associated with homoclinic orbits. Symmetry factors also must be included if one is to obtain a quantitatively correct picture of scarring.

III. LINEAR THEORY OF SCARRING

For completeness and context we need to review the linear theory of scarring, first discussed in Ref. [3]. Consider an unstable fixed point of a classical map located at the origin, with the stable and unstable manifolds oriented along the p (vertical) and q (horizontal) axes, respectively. (We will adopt this choice of coordinate system throughout. In general, a canonical transformation needs to be performed, *e.g.* in the case of an inverted harmonic oscillator, to rotate and skew the stable and unstable manifolds into this alignment). Linearizing the map around the fixed point, we obtain to first order

$$\begin{aligned} q' &= e^{\lambda t} q \\ p' &= e^{-\lambda t} p \,, \end{aligned} \tag{1}$$

where λ is the Lyapunov exponent for one iteration of the orbit. (The situation is very similar in the case where the stable and unstable manifolds are not thus aligned, and analogous formulae can be derived for that scenario. Also, for simplicity we do not discuss the case of a wavepacket centered near, but not on, a periodic orbit (see Ref. [3]).) We now take a gaussian wavepacket

$$g_\sigma(q) = (\frac{4\pi\hbar^2}{\sigma^2})^{1/4} e^{-q^2/2\sigma^2} \,, \tag{2}$$

which corresponds to a classical distribution centered on the origin with width σ in the q direction and width $\sigma_p = \hbar/\sigma$ in the p direction ($\hbar \ll \sigma \ll 1$, *e.g.* $\sigma \sim \sqrt{\hbar}$). Now for a small enough $\hbar$, the initial wavepacket and its short-time iterates are contained within the linear regime, and we have the time-evolved wavepacket $g_t(q) = U^t g_\sigma(q)$ given by the expression above in Eq. 2 with σ replaced by $\sigma_t = e^{\lambda t}\sigma$ (here U is a quantum operator corresponding locally to the classical dynamics given by Eq. 1). Classically this corresponds to a horizontal stretching and vertical shrinking of the gaussian distribution in phase space.

The overlap

$$A(t) = \langle g_t | g \rangle = \frac{e^{i\theta t}}{\sqrt{\cosh(\lambda t)}} \tag{3}$$

is easily found by Gaussian integration (notice that the autocorrelation function $A(t)$ is independent of σ, the width of the initial wavepacket). Here θ is the quantum phase associated with the fixed point (semiclassically it is given by $S/\hbar$, S being the action for one traversal of the periodic orbit, plus Maslov phases arising from caustics). This time domain behavior can be fourier transformed to obtain an envelope in the (quasi-)energy spectrum, centered at $E = \theta$ and with a width which depends only on λ, scaling linearly with λ for small λ.

We remark here that the situation for a fixed point of period $P > 1$ is similar. In this case the linear autocorrelation function is nonzero only at integer multiples of P, and the corresponding spectrum has P identical bumps, each of a width and height related to the instability of the entire orbit (see also the discussion in Section VIII B). Additional time scales are present in a continuous-time system, which are not directly relevant to the phenomenon of scarring,

but which produce a background spectrum relative to which scarring can manifest itself. These issues are addressed in Section VII B of this paper.

In the case of exact linearity, or where the evolving wavefunctions are allowed to escape to infinity at long times (as in an inverted harmonic oscillator), the preceding is all that there is to be said about the spectrum of the wavepacket. The width of the spectral bump then corresponds to a decay rate. But in a closed, unitary system, the escaping probability must eventually start returning to the origin. In a classically mixing system, this will begin happening not later than by the mixing time, this being the time required for a classical distribution corresponding to a minimum uncertainty wavepacket to spread through all of phase space on a mesh of size $\hbar$. The mixing time scales as $T_{\rm mix} \sim \log_{\overline{\lambda}}(N)$, where $\overline{\lambda}$ is the "typical" exponent for the entire system, and N is the total number of states in the available phase space.

The key point is that the Fourier transform of $A(t)$ for small λ localizes the spectrum (local density of states) to a region of width $\sim \lambda$, smaller than the whole quasi-energy interval. In effect the initial state is in a resonance mode which decays more slowly than a random state. A random state should decay in a time of the order of a single time step for a discrete map. (The reason for the single step decay is simple: a random state having a random (*i.e.* RMT) local density of states spectrum has a quasi-energy uncertainty of the whole interval ($\delta\epsilon = \delta\omega/\hbar = 2\pi$). Now $\hbar\delta\epsilon\delta\tau \sim \delta\omega\delta\tau \sim \hbar$ implies $\delta\tau \sim \mathcal{O}(1)$, *i.e.* one time step). The corresponding resolved spectrum for a wavepacket launched on a periodic orbit thus *cannot* be picked from an *a priori* RMT local density of states, as Figure 1 shows. Now, to complete the point, we recall that the spectral line intensities are the squared projections of eigenstates onto the local "test" Gaussian. *The intensities are the "support" of the envelope, and are thus required to be (upon local average) larger in the peak region of the envelope than RMT predicts by a factor of order* λ^{-1}. This enhancement of the overlaps (that is, the enhancement by a factor of order λ^{-1} over the statistical expectation of $1/N$, where N is the dimension of the Hilbert space) means that at a minimum there must be states with a projection onto the test state of order λ^{-1} larger than what is statistically expected. However, if this projection were to be shared in an egalitarian fashion among all the available states, then most or all of the states in the peak region would be enhanced by this factor. On the other hand, if only a small fraction f of the available states are enhanced, then these states must have larger projections $\mathcal{O}(\lambda^{-1}f^{-1})$ onto the test state in order to support the local density of states envelope. These two extremes are illustrated in Figure 2. The short time dynamics, which depends only on the linear or "tangent" map around the periodic orbit on which the test Gaussian is centered, cannot tell us without further assumptions which extreme (or intermediate) regime is realized; it only tells us that some states must be enhanced. The egalitarian case corresponds to the least striking type of scarring, since each state is enhanced at most by a factor of order λ^{-1}. If λ is not too small, this enhancement is not even competitive with the fluctuations expected from RMT, and we might conclude by cursory inspection that individual states are not scarred at all. Indeed, this would be a justifiable definition, although the *systematic*, statistically significant enhancement of many nearby states in the egalitarian case would still reveal the underlying mechanism of scar localization. In effect this definition was adopted by Steiner and co-workers [13] in their studies of the eigenstates of the hyperbolic billiards, which appear to live close to the egalitarian limit. In the opposite "totalitarian" extreme, enhancements are very large, and scars are obvious in pictures of eigenstates, even for orbits which are very unstable. It is important to note however that for small λ even the linear (short time) theory in the "worst case" egalitarian scenario predicts strong scarring, well above the typical RMT fluctuations, of strength $1/\lambda$.

These considerations extend easily to include the possible dependence of scar strength on $\hbar$ or on the density of states. If the density of states is such that only one or a few states can exist within a quasi-energy width λ, then effectively only the "totalitarian" option exists. This is a strong localization regime, where one or a few states carry the total scar intensity. At the ideal unitary limit of an overlap of 1, one state is entirely localized to the periodic orbit region. (This was the basis for our conclusion that the bouncing ball modes in the stadium billiard persist up to infinite energy [19]). Starting from this extreme, as N increases, the scar strength of individual eigenstates *could* decrease as fast as $1/N$, in the egalitarian limit, although the intensity *enhancement factor* would still remain finite, as the average intensity is also decreasing as $1/N$. (In a billiard system there is a $\sqrt{E}$ increase in the number of affected states with increasing E: the density of states is independent of E but the energy width δE of the scar "resonance" scales as $\sqrt{E}\lambda$, where again λ is the Lyapunov exponent for a complete period of the orbit. The time required to traverse this orbit goes as $1/\sqrt{E}$, thus $\delta E \sim \sqrt{E}\lambda$).

We remark that scarring can become no weaker than the egalitarian limit defined above for any given periodic orbit, even as $\hbar \to 0$. Suppose that the egalitarian limit is the usual circumstance as $\hbar \to 0$. Then scars become less dramatic but do not disappear as $\hbar \to 0$ as measured by the test states whose area in a surface of section is h. However this area (projected onto coordinate space, say) amounts to a diminishing portion (going as $\sqrt{\hbar}$ for a phase space Gaussian with an aspect ratio of order unity) of the total coordinate space volume. These subtleties have caused much confusion over whether scars "disappear" as $\hbar \to 0$.

A. Husimi projections and phase space tubes

The projection of Gaussian wavepackets, or other distributions localized around periodic orbits, onto the eigenstates as a test of their localization properties was introduced in Ref. [3]. Subsequently, the idea of detecting and quantifying scars by integrating over tubes in phase space surrounding the periodic orbit has been discussed [15]. The tube should be of diameter $\sqrt{\hbar}$ normal to the direction of the orbit. The diameter originally used was $\hbar$ but $\sqrt{\hbar}$ is more appropriate and is used in more recent work (S. Fishman, private communication). Of course, the structure of the linear local dynamics around the periodic orbit must also be considered here. In particular, for certain alignments of the stable and unstable manifolds with respect to the p and q directions, a tube of width $\hbar$ in position space and width 1 in momentum would be equally optimal. This is consistent with the findings of Li [22], where certain orbits in a stadium billiard show optimal scarring in coordinate space with a tube size scaling as the wavelength (instead of as the square root of the wavelength).

The phase space tube approach is closely related to the Gaussian wavepacket projection, as we shall now show. In two dimensions, suppose we average the Gaussian projections over the whole length of the periodic orbit (instead of taking an overlap with a Gaussian centered at just one periodic point). The mean wavepacket momentum points along the orbit. Then we have, for an orbit pointing along the x-axis, the average projection S given by

$$S = \frac{1}{L_x}\int dx_0 |\langle \alpha(x_0, p_{x0}, y_0, 0)|\psi_E\rangle|^2 = \mathrm{Tr}(\rho_L|\psi_E\rangle\langle\psi_E|)\,, \tag{4}$$

where

$$\begin{aligned}\rho_L(x,y,x',y') = \frac{1}{L_x}\int dx_0 \exp[&-(x'-x_0)^2/2\sigma_x^2\hbar - (x-x_0)^2/2\sigma_x^2\hbar \\ &-(y'-y_0)^2/2\sigma_y^2\hbar - (y-y_0)^2/2\sigma_y^2\hbar + i(x-x')p_{0x}/\hbar] \\ \sim \exp[&-(x'-x)^2/4\sigma_x^2\hbar - (y'-y_0)^2/2\sigma_y^2\hbar - (y-y_0)^2/2\sigma_y^2\hbar + i(x-x')p_{0x}/\hbar]\,.\end{aligned} \tag{5}$$

Now we Wigner transform this density matrix:

$$\begin{aligned}\rho_L^W(\mathbf{q},\mathbf{p}) &= 2^d \int_{-\infty}^{\infty} e^{-2i\mathbf{p}\cdot\mathbf{s}/\hbar}\rho_L(\mathbf{q}+\mathbf{s},\mathbf{q}-\mathbf{s})\,\mathrm{d}\mathbf{s} \\ &= \rho_L^W(x,p_x;y,p_y) \sim \exp\left[-(y-y_0)^2/\sigma_y^2\hbar - \sigma_y^2(p_y-p_{y_0})^2/\hbar - \sigma_x^2(p_x-p_{x_0})^2/\hbar\right].\end{aligned} \tag{6}$$

We see *this is a phase space tube surrounding the classical trajectory, of diameter* $\propto\sqrt{\hbar}$, if σ_y^2, the aspect ratio in the y–p_y subspace, is chosen to be of order unity. Hence, the relation between the Fishman *et al.* phase space tube and the Husimi projection is that the tube is the Husimi projection averaged over the entire length of the orbit. The advantage of this smearing is the same as its disadvantage: it is insensitive to the local direction of the classical invariant manifolds. In this sense the tube is a somewhat duller probe for scarring, while at the same time it has the advantage of providing a more universal description of scars.

B. Limitations of the linear theory

If the initial periodic orbit is sufficiently unstable, a "quiet time" regime may exist after the linear autocorrelation function has decayed and before the nonlinear recurrences have had a chance to build up. This effect is not included in the linear theory and will be reflected in the absence of features in the spectrum corresponding to these time scales. (See also the discussion in section VII B.) In the semiclassical limit, however, the quiet time is very short compared to the Heisenberg time $T_H \sim N$, where individual eigenvalues begin to be resolved, and where the quantum mechanics begins to be quasiperiodic. (At time T_H the information contained in the quantum mechanics gets exhausted, and the autocorrelation function at longer times can be reconstructed using only the information for times up to T_H.) Nonlinear recurrences at times between the end of the quiet time regime and the onset of Heisenberg-scale dynamics are crucial for a proper understanding of scarring, and will be the subject of Section V of this paper.

This section has been a review of the "existing" theory with remarks aimed at more recent work. There are shortcomings of this theory which we aim to remedy below:

- The linear theory does not say how the localization, predicted from the short time dynamics, actually manifests itself in the long time behavior of the autocorrelation function $A(t)$.

- The linear theory can have no information about whether the totalitarian or egalitarian limit of scar intensity distribution over the available eigenstates is approached. This information comes from longer time dynamics which necessarily involves more than the linearized tangent map of the periodic orbit.
- No systematic study of scar strength over a large enough ensemble to unambiguously test the predictions of the linear theory has yet been undertaken.

IV. SCARRING AS A LOCALIZATION PHENOMENON

It is well known that short time coherences in amplitudes lead to weak localization effects. An example is provided by coherent backscattering in random media, where a factor of 2 enhancement is realized from the fact that a quantum path and its time reversed image contribute equally, with the same phase. Ensemble averaging cannot remove this effect.

Scarring also involves a weak localization effect resulting from short time correlations which depend on the properties of classical *unstable* periodic orbits, and also symmetry, with consequences similar to those of coherent backscattering. The short time coherences have an effect on the long-time, stationary properties. In the time domain, this means that the return probability at long times for an initial state launched on an unstable periodic orbit is enhanced from what one would expect naively in the absence of this classical information. In the energy domain, a wavepacket located near a periodic orbit will have enhanced, non-random overlaps with the available eigenstates of the system. These enhanced overlaps imply that scarring exists, although there is a subtle issue of how the "scar strength" is to be shared amongst the eligible eigenstates. This issue of scar sharing is key to understanding the strength of scars in individual eigenstates. We will describe briefly the concept of weak localization from the time and energy points of view and the connection between them (A fuller discussion can be found in Ref. [23]), and then go on to discuss how such an effect can arise from short-time classical behavior.

Consider a compact classical phase space of area A, with chaotic dynamics given by a discrete-time evolution (area-preserving map of A onto itself), and no conserved quantities. A two-dimensional billiard can be reduced to such a discrete time one-dimensional map by the surface of section technique. (Although we restrict ourselves to one spatial dimension for specificity, the concepts are completely generalizable.) Our results can be extended to a situation in which conserved quantities (such as energy) are present, by considering flow between phase space-localized states (usually coherent states), and taking account of the energy spread contained in such states. This problem is treated in Ref. [28], and is also mentioned briefly in SectionVII B of this paper. We will assume in the present discussion that all of phase space is classically accessible from any smooth starting distribution.

If the area is an integer multiple of Planck's constant h, $A = Nh$, the system can be quantized (with a choice of quantization conditions), to obtain an N-dimensional Hilbert space. Because the underlying classical dynamics is completely ergodic, one might expect the eigenstates to appear random in any natural basis, such as that of position, momentum, or Gaussian states. Thus, let $|a\rangle$ be such a physically-motivated basis and $|n\rangle$ be the basis of eigenstates. Then we expect the overlaps $f_{an} = \langle a|n\rangle$ to be Gaussian variables with the normalization condition $< |f_{an}|^2 >= 1/N$. This does *not* mean that all energy eigenstates have equal overlaps with all the trial basis states, *i.e.* $|f_{an}|^2 \neq 1/N$ for all a, n. In fact, such a Gaussian distribution (predicted by random matrix theory, which is based on the absence of a preferred basis for analyzing the dynamics), leads to $< |f_{an}|^4 >= F/N^2$, where $F = 3$ if both $|a\rangle$ and $|n\rangle$ are real (convenient if, for example, the dynamics is time-reversal invariant), and $F = 2$ otherwise. This is a quantum fluctuation result and is already a deviation from the classical expectation of $F = 1$. Localization, however, is taken to mean an additional deviation of the f_{an} distribution, away from Gaussian form, towards a distribution with a longer tail. In particular, the inverse participation value (IPR) $< N^2|f_{an}|^4 >$ (where the average can be taken over trial states, energy eigenstates, or both, and also over an ensemble of systems) is in the presence of such localization enhanced from its ergodic value of F. Higher moments and the behavior of the tail can also be investigated.

An important point is that scars entail a correlation between overlap probabilities $|f_{an}|^2$ and the energies E_n, for a wavepacket $|a\rangle$ located on a periodic orbit (such correlations are absent under the assumptions of RMT). In fact, in the case of random new long-time recurrences superimposed on top of semiclassically understood short-time dynamics, the distribution of f_{an} overall and as a function of E_n can be predicted analytically, in terms of that short-time dynamics, as will be shown below in Section VI.

Let us now consider the connection with the time domain. We define the autocorrelation function $A(t) = \langle a|U^t|a\rangle$, where U is the discrete time evolution operator (a completely analogous notation can be written down for continuous time). The fourier transform of $A(t)$ is the weighted spectrum (local density of states) $S(E) = \sum_n \delta(E - E_n)|f_{an}|^2$. The squared autocorrelation function

$$|A(t)|^2 = \left| \sum_n |f_{an}|^2 e^{-iE_n t} \right|^2 \tag{7}$$

can be thought of as a wavepacket-specific form factor, similar to the usual spectral form factor $F(t) = \sum_{mn} e^{-i(E_n - E_m)t}$, but weighting each term by the heights of the corresponding lines in the spectrum $S(E)$ above.

For long times, in the absence of degeneracies, one easily obtains the relation

$$\begin{aligned} < |A(t)|^2 >_t \; &\equiv \lim_{T_{\max}\to\infty} \frac{1}{T_{\max}} \sum_{t=0}^{T_{\max}-1} |A(t)|^2 \\ &= \sum_n |f_{an}|^4 \,, \end{aligned} \tag{8}$$

where on the left hand side a time average must be taken over times long compared to the Heisenberg time T_H (generically $T_H \sim N$). Within RMT, both sides of Eq. 8 are predicted to approach F/N, in the semiclassical limit $N \to \infty$. Localization is associated with an enhancement in the long-time return probability $< |A(t)|^2 >_t$. We will see in Section V how this is possible in the case of scarring. We will also see there that short-time unstable orbits induce nontrivial correlations $< A^*(t+\Delta)A(t) >$ at long times t. These will be seen to correspond to eigenvalue-eigenstate correlations (through the formation of an envelope in the spectrum) in the energy domain.

V. BEYOND THE LINEAR THEORY

A. Homoclinic orbits

In keeping with our treatment of the linear theory of scarring, we will now discuss long time recurrences in the autocorrelation function from a semiclassical point of view. Let us consider a homoclinic orbit which begins near the fixed point $(0,0)$ along the unstable manifold at large negative times and again approaches the fixed point along the stable manifold at large positive times. Specifically, let the orbit $\mathcal{HC}$ be given by $\{(q_t, p_t)\}_{t=-\infty\ldots\infty}$, such that $(q_t, p_t) = (ae^{\lambda t}, 0)$ for $t \to -\infty$ and $(q_{t'}, p_{t'}) = (0, be^{-\lambda t'})$ for $t' \to +\infty$. Then we claim that a thin vertical strip cut out of the initial Gaussian near $q = ae^{\lambda t}$ at time t will intersect the same Gaussian as a long horizontal strip at $p' = be^{-\lambda t'}$ at a much later time t'. Note that because the wavepacket is contained well inside the linearizable region around the fixed point, the dynamics from time t to time t' can be divided into three parts. First, the tall, narrow distribution shrinks vertically and stretches horizontally as its center moves out horizontally at an exponential rate along the unstable manifold (for, let us say, τ_1 steps). This is followed by complicated nonlinear dynamics which eventually brings the center of the distribution back into the linearizable region, this time along the stable manifold of the fixed point. Now the part of the distribution which is in the linear region again begins to stretch horizontally and shrink vertically, becoming a narrow horizontal strip moving in towards the original wavepacket. We will denote by τ_3 the time spent in this last stage of the evolution. The first and third parts of the dynamics allow the breadth of the initial distribution centered on $(ae^{\lambda t}, 0)$ and the height of the final distribution centered on $(0, be^{-\lambda t'})$ both to be small compared to the size of the Gaussian wavepacket. All of this is illustrated in Figure 3.

The overlaps of the Gaussian with the vertical and horizontal strips, as well as the effects of the linear dynamics in stages one and three are easy to write down analytically. There is also an amplitude factor Q which measures the stretching of the distribution in the nonlinear stage of the dynamics, from time $t + \tau_1$ until time $t' - \tau_3$. Finally, there is a phase ϕ_{nonlin} associated with this nonlinear excursion. The total contribution to the wavepacket autocorrelation function at time $t' - t$ coming from this homoclinic excursion is given by a product of five factors:

$$A_{\mathcal{HC}} = e^{-q_t^2/2\sigma^2} \cdot e^{i\tau_1\theta} e^{-\lambda\tau_1/2} \cdot Q(t+\tau_1, t'-\tau_3) e^{i\phi_{\text{nonlin}}} \cdot e^{i\tau_3\theta} e^{-\lambda\tau_3/2} \cdot e^{-p_{t'}^2/2\sigma_p^2} \,. \tag{9}$$

The factors $e^{-\lambda\tau_1/2}$ and $e^{-\lambda\tau_3/2}$ are instability factors associated with the linearized motion of the wavepacket, while $e^{i\tau_1\theta}$ and $e^{i\tau_3\theta}$ are the corresponding phases. The suppression factors $e^{-q_t^2/2\sigma^2}$ and $e^{-p_{t'}^2/2\sigma_p^2}$ are associated with the fact that the initial and final points of the excursion are both off-center relative to the gaussian wavepacket. The total correlation function $A(T)$ is given semiclassically by a sum of terms of the form given above over all homoclinic excursions of length $t' - t = T$.

$$A_{\text{SC}}(T) = \sum_{\mathcal{HC}} \delta_{t'_{\mathcal{HC}} - t_{\mathcal{HC}} - T} A_{\mathcal{HC}} \,. \tag{10}$$

B. Effect of short-time dynamics

One might think naively that the various contributions to the sum in Eq. 10 are all independent and uncorrelated at long times, but this is not the case. In fact, correlations are present both among the different contributions to the autocorrelation function at a fixed time, and also among homoclinic contributions of different excursion lengths T. Let us consider the homoclinic orbit of the previous subsection, with the mapping taking us from $(ae^{\lambda t}, 0)$ to $(0, be^{-\lambda t'})$ in the time interval $T = t' - t$. Now of course the same homoclinic orbit takes the Δ_1-step iterate of the original point, $(ae^{\lambda(t+\Delta_1)}, 0)$ to the Δ_3-step iterate of the final point, $(0, be^{-\lambda(t'+\Delta_3)})$, in a time $T + \Delta_3 - \Delta_1$. In particular, taking $\Delta_1 = \Delta_3$, we have a family of excursions, all of the same length, associated with one homoclinic orbit. An important thing to notice is that all these contributions come with the same phase, the extra phase in the final Δ_3 steps approaching the fixed point being exactly canceled by the missing Δ_1 steps at the beginning of the trip (there is only one phase associated with the fixed point, and it is the same in stages one and three). ("1" and "5" in Figure 3 have exactly the same phase relation as "2" and "6".) The phase $\phi_{\rm nonlin}$ coming from the nonlinear dynamics in stage two is, of course, independent of $\Delta_{1,3}$. Naturally, the exponential prefactor

$$\begin{aligned} & e^{-q_{t+\Delta_1}^2/2\sigma^2} e^{-p_{t'+\Delta_3}^2/2\sigma_p^2} e^{-\lambda(\tau_1-\Delta_1)/2} e^{-\lambda(\tau_3+\Delta_3)/2} \\ & = e^{-(q_t e^{\Delta_1\lambda})^2/2\sigma^2} e^{-(p_{t'} e^{-\Delta_3\lambda})^2/2\sigma_p^2} e^{-\lambda(\tau_1-\Delta_1)/2} e^{-\lambda(\tau_3+\Delta_3)/2} \end{aligned} \tag{11}$$

will depend on $\Delta_{1,3}$, so only a finite number of the infinite family of contributions for $\Delta_1 = \Delta_3$ will be of significant size (this number, the number of iterations for which one tends to stay near the periodic orbit, scales as $1/\lambda$.) However, all of these will add exactly in phase. This is an important difference between the classical and semiclassical long-time dynamics of the system. The presence of this coherence is the underlying reason for the fact that in quantum mechanics the probability for coming back to an unstable periodic orbit at long times is enhanced over the classical value of $1/N$, which fact leads to scarring in the eigenstate domain, as seen in Section IV.

We also notice that if we take $\Delta_1 \neq \Delta_3$, so the new excursion length is different from the original one, the difference in phase is given by $e^{i\theta(\Delta_3-\Delta_1)}$, and each excursion of length T also contributes to the autocorrelation function at $T+\Delta \equiv T+\Delta_3-\Delta_1$, with this extra phase and a somewhat different amplitude prefactor. Thus, as will be explained in more detail in the following section, nontrivial correlations will be present in the autocorrelation function at nearby times, $< A^*(T+\Delta)A(T) >$, for small Δ. This is an effect that is qualitatively easy to understand even in a classical picture in terms of a "reloading" of the original wavepacket. Because the original wavepacket is centered on a fixed point of the map, any significant recurrence at time T is expected to be accompanied by a recurrence for all times $T + \Delta$, where Δ is within the decay time associated with the fixed point. In effect, any new long-time recurrences get convoluted with the (linear) short-time dynamics of the system around the fixed point. In the energy domain, this corresponds (by fourier transform) to a *multiplication* of the original linear envelope by an oscillating function associated with the long-time recurrence. In the following section, these statements will be made more explicit and quantitative under the assumption of randomness in the homoclinic orbits which lead to long-time recurrences.

VI. RANDOM RECURRENCE MODEL

A. Correlations among homoclinic excursions

In a chaotic system, the number of homoclinic orbits increases exponentially with the excursion length at long times. Let us for the moment assume that the nonlinear phases associated with the terms in Eq. 10 are uncorrelated at long times. We also assume a uniform distribution of homoclinic points q_t and $p_{t'}$ along the unstable and stable manifolds. We then obtain for the average square of the long-time semiclassical autocorrelation function

$$< |A_{\rm SC}|^2 >_{\rm diag} = \mathcal{N} \int dq_t \int dp_{t'} e^{-q_t^2/\sigma^2} e^{-p_{t'}^2/\sigma_p^2}\,, \tag{12}$$

where the "diag" subscript indicates that we are working in a diagonal approximation (no correlations between the homoclinic orbits). The mean squared amplitude factor associated with the excursions as well as the densities of homoclinic points along the two manifolds have been incorporated into the normalization factor $\mathcal{N}$. This normalization factor can easily be fixed by noticing that classically, in the absence of any coherence effects, the return probability must approach $1/N$ at long times.

We now correct the assumption made in the previous paragraph and include the fact that, as discussed in the preceding section, the contributions from homoclinic excursions associated with a single homoclinic orbit all add in phase. We then have

$$< |A_{\rm SC}| >^2 = \mathcal{N}' \int dq_t \int dp_{t'} \left| \sum_{\Delta_1} e^{-(q_t e^{\Delta_1 \lambda})^2/2\sigma^2} e^{-(p_{t'} e^{-\Delta_1 \lambda})^2/2\sigma^2} \right|^2 , \tag{13}$$

where the normalization factor $\mathcal{N}'$ is given by

$$< |A_{\rm SC}| >^2_{\rm diag} = \mathcal{N}' \int dq_t \int dp_{t'} \sum_{\Delta_1} \left| e^{-(q_t e^{\Delta_1 \lambda})^2/2\sigma^2} e^{-(p_{t'} e^{-\Delta_1 \lambda})^2/2\sigma^2} \right|^2 = 1/N \, . \tag{14}$$

We now see that the enhancement factor $< |A_{\rm SC}| >^2 / < |A_{\rm SC}| >^2_{\rm diag}$ is given by

$$\begin{aligned} &\frac{\sum_{\Delta_1, \tilde{\Delta}_1} \int dq_t \int dp_{t'} g_{\tilde{\Delta}_1}(q_t, p_{t'}) g_{\Delta_1}(q_t, p_{t'})}{\sum_{\tilde{\Delta}_1} \int dq_t \int dp_{t'} g_{\tilde{\Delta}_1}(q_t, p_{t'}) g_{\tilde{\Delta}_1}(q_t, p_{t'})} \\ &= \frac{\sum_{\Delta_1} \int dq_t \int dp_{t'} g_{\tilde{\Delta}_1}(q_t, p_{t'}) g_0(q_t, p_{t'})}{\int dq_t \int dp_{t'} g_0(q_t, p_{t'}) g_0(q_t, p_{t'})} , \end{aligned} \tag{15}$$

where g_0 is a Gaussian distribution of width σ in position and σ_p in momentum, and g_{Δ_1} is the same distribution stretched by a factor of $e^{\Delta_1 \lambda}$ horizontally and compressed vertically by the same factor. In Eq. 15 we have used the relations

$$\int dq_t \int dp_{t'} g_{\tilde{\Delta}_1}(q_t, p_{t'}) g_{\tilde{\Delta}_1}(q_t, p_{t'}) = \int dq_t \int dp_{t'} g_0(q_t, p_{t'}) g_0(q_t, p_{t'}) \tag{16}$$

and

$$\int dq_t \int dp_{t'} g_{\tilde{\Delta}_1}(q_t, p_{t'}) g_{\Delta_1}(q_t, p_{t'}) = \int dq_t \int dp_{t'} g_{\tilde{\Delta}_1 - \Delta_1}(q_t, p_{t'}) g_0(q_t, p_{t'}) \, . \tag{17}$$

Returning to the discussion following Eq. 2 we notice that the overlap of the original Gaussian wavepacket $a(q)$ with the same wavepacket stretched by a factor $e^{\Delta_1 \lambda}$ is just the linearized autocorrelation function $A_{\rm lin}(\Delta_1)$. The overlap of the corresponding classical distributions is given by $|A_{\rm lin}(\Delta_1)|^2$, and finally we have

$$< |A_{\rm SC}| >^2_{\rm coherent} = \frac{1}{N} \sum_{\Delta_1} |A_{\rm lin}(\Delta_1)|^2 \, . \tag{18}$$

A similar analysis can be performed for the case $\Delta \equiv \Delta_3 - \Delta_1 \neq 0$, and there we find

$$< A^*(T + \Delta) A(T) >_{\rm coherent} = \frac{1}{N} \sum_{\Delta_1} A^*_{\rm lin}(\Delta + \Delta_1) A_{\rm lin}(\Delta_1) \, . \tag{19}$$

This shows the unmistakable effect of the short-time correlations at long times. The expressions obtained here quantify the connection between short-time and long-time behavior which was already suggested in the previous section.

B. Reloading: another point of view

We can also understand the results of Eqs. 18,19 in a somewhat different way, as suggested by the "reloading" picture of Section V B. We write $A(T)$ at long times as

$$\begin{aligned} A(T) &= A_{\rm new}(T) + A_{\rm reloaded}(T) \\ &= A_{\rm new}(T) + \sum_{\Delta \neq 0} A_{\rm new}(T - \Delta) A_{\rm lin}(\Delta) \, , \end{aligned} \tag{20}$$

where $A_{\rm new}(T)$ are random, uncorrelated Gaussian variables with variance $1/N$, *i.e.* $< A^*_{\rm new}(T') A_{\rm new}(T) >= \delta_{TT'} \frac{1}{N}$ in an ensemble average. Then one easily obtains the results of Eqs. 18,19. The assumption being made here is that the new amplitude coming back to the fixed point at long times fills the original Gaussian evenly in an unbiased way, so that the evolution of this newly returned amplitude is equivalent to the evolution of the original Gaussian. We saw above that this is rigorously true semiclassically for uncorrelated homoclinic orbits. However, the picture

presented here may apply also to situations where large short-time recurrences arise for reasons other than periodic orbits. These recurrences may be due to "almost periodic orbits", *i.e.* classical orbits that return to within a minimum uncertainty wavepacket of the starting point in phase space. Localization effects due to short-time recurrences arising from diffractive paths ("diffractive scarring") may also be understandable in this general framework.

It is important to point out that the reloading idea is critically dependent on the hyperbolic nature of the dynamics. With a bit of coarse graining hyperbolicity quickly erases certain information about location in phase space. More specifically, the attraction of orbits to the unstable manifolds means that location along the contracting directions is relatively unimportant.

C. Effect on spectra

We now claim that the time domain correlations given in Eq. 19 are just the right correlations to produce spectral fluctuations which multiply the original linear envelope. (This is important because one might have thought that the oscillations in the spectrum caused by long-time recurrences simply get added to the original linear envelope, instead of multiplying it. This would produce completely different spectral behavior on small energy scales.) Indeed suppose the spectrum has the form

$$S(E) = S_{\rm lin}(E) S_{\rm fluct}(E)\,, \tag{21}$$

where $S_{\rm lin}(E) = 2\pi \sum_T e^{iET} A_{\rm lin}(T)$ is the spectrum given by the linear dynamics, and $S_{\rm fluct}(E)$ is the fluctuating part, with the property that $K \equiv < |S_{\rm fluct}(E)|^2 >$ is an $E-$independent constant (an ensemble average is implied in the definition of K). Now we have

$$< A^*(t+\Delta)A(t) > = < \int dE' S^*_{\rm lin}(E') S^*_{\rm fluct}(E') e^{iE'(t+\Delta)} \int dE S_{\rm lin}(E) S_{\rm fluct}(E) e^{-iEt} > \ . \tag{22}$$

Averaging over t, and inserting the expression for $S_{\rm lin}(E)$ from above,

$$\begin{aligned} < A^*(t+\Delta)A(t) > \ &= < 2\pi \int dE |S_{\rm lin}(E)|^2 |S_{\rm fluct}(E)|^2 e^{iE\Delta} > \\ &= < \frac{1}{2\pi} \int dE |S_{\rm fluct}(E)|^2 e^{iE\Delta} \sum_{TT'} e^{iE(T'-T)} A^*_{\rm lin}(T') A_{\rm lin}(T) > \ . \end{aligned} \tag{23}$$

Finally, inserting the fluctuation intensity K and performing the energy integral, we obtain

$$< A^*(t+\Delta)A(t) > = K \sum_T A^*_{\rm lin}(T+\Delta) A_{\rm lin}(T)\,, \tag{24}$$

which agrees with the result in Eq. 19 above, obtained by taking into account the phase coherence of all the homoclinic excursions associated with a single homoclinic orbit.

D. Heisenberg time dynamics and symmetries

Up until now we have been assuming that the nonlinear recurrences associated with the homoclinic orbits are sums of random contributions, under the constraint of correlations due to the short-time linear behavior near the periodic orbit. The picture here is that random "new" recurrences get smeared out by a function associated with the reloading effect. This leads to Gaussian random fluctuations in the spectrum at all scales short compared to the inverse of the mixing time, all of these uncorrelated fluctuations multiplying the initial linear envelope. But now we have to include an additional constraint coming from Heisenberg time dynamics, namely unitarity and discreteness of the spectrum. In the absence of scarring, these long-time correlations cause the mean return probability $|A_{\rm QM}(t)|^2$ to converge to a value of $2/N$ at long times, $3/N$ if the eigenstates and the initial wavepacket are both purely real. We may reasonably suppose that this long-time constraint, associated with the statistics of very long excursions away from the periodic orbit, is independent of the short-time behavior near the periodic orbit. Thus, if we suppose that what we in the previous section called stage two of the dynamics does not know about the trajectory's approach to the periodic orbit at times $|t| \to \infty$, then the same long-time constraints should be present in the case of scarring. So we finally obtain a discrete spectrum, with intensities given by a χ^2 variable of 2 degrees of freedom (1 degree of freedom for purely

real f_{an}), except that in the case of scarring this RMT line spectrum multiplies the original short-time envelope. The line height associated with energy E_n is given by

$$|f_{an}|^2 = \frac{1}{N} S_{\rm lin}(E_n) |r_n^2| \,, \tag{25}$$

where r_n is a Gaussian variable, real or complex, with variance one. In particular, the first two moments of this distribution are given by

$$< |f_{an}|^2 >= \frac{1}{N} S_{\rm lin}(E_n) \quad < |f_{an}|^4 >= \frac{F}{N^2} S_{\rm lin}^2(E_n) \,, \tag{26}$$

where $F = 2$ or 3 as explained above. We may note here that the linear spectrum $S_{\rm lin}(E)$ is purely real because of the unitarity of the time evolution, $A(-t) = A^*(t)$. This holds also for the full spectrum $S(E)$, and for any smoothed spectrum obtained by fourier transforming $A(t)$ for all times $|t| < T_{\rm max}$.

The inverse participation ratio for the wavepacket is given by

$$\begin{aligned} N < \sum_n |f_{an}|^4 > \; &= F \int dE \; S_{\rm lin}^2(E) \\ &= F \sum_T |A_{\rm lin}(T)|^2 \\ &= F \sum_T [\cosh(\lambda T)]^{-1} \\ &\to cF/\lambda \;\; \text{for small} \;\; \lambda \,. \end{aligned} \tag{27}$$

Note that the IPR enhancement factor is a number that depends only on the Lyapunov exponent of the periodic orbit. Higher moments of the f_{an} distribution can be computed easily in terms of $A_{\rm lin}(T)$, always taking into account the proper quantum fluctuation factors.

If the spectrum $S(E)$ is ensemble-averaged while preserving the periodic orbit (*i.e.* if we average over the nonlinear dynamics only), we recover the original linear envelope spectrum, the same spectrum which is present in the case of an open system.

Finally we need to mention here an issue that has been the cause of some misunderstanding in the literature, namely the issue of spatial symmetries. In symmetric systems like the stadium billiard, many periodic orbits either remain invariant under a reflection operation, or they get shifted by some fraction of the total period, or else they get mapped to their time-reversed counterparts. In all these cases, one expects extra correlations in the contributions coming from the homoclinic excursions which are related by such a symmetry operation. Thus, consider the simplest case of a parity symmetry, where the initial wavepacket centered on the periodic orbit remains unchanged under the symmetry. Of course we know from quantum mechanics that the wavepacket can overlap only with states in the even part of the Hilbert space, so the IPR is increased by a factor of two from the value that would otherwise be expected. We can also see this effect semiclassically, because each homoclinic excursion away from the invariant periodic orbit has a counterpart related by parity, and the contributions from the two have the same amplitude and phase, so they add constructively. More complicated situations can be treated similarly, and we will not go into the details here. In the example described later in the paper, in Section IX, we have intentionally desymmetrized the system of interest to eliminate the enhanced scarring effects.

VII. HIERARCHY OF SPECTRAL ENVELOPES

In the previous section, we have constructed a model in which an initial linear envelope is multiplied by random fluctuations associated with scales between the mixing time and the Heisenberg time, producing a discrete spectrum with heights that have a Porter-Thomas distribution multiplying a smooth envelope. In this section, the picture will be extended to incorporate other time scales that may be present in the system.

A. Isolated recurrences

Suppose an isolated homoclinic orbit exists which leads to an anomalously large return amplitude at some time $T_{\rm isol}$ which is large compared to the decay time of the linear evolution. If $T_{\rm isol}$ is also small compared to the time at which

the returning orbits begin to proliferate exponentially, we obtain a hierarchy of scales in the spectrum. The initial linear envelope of width $2\pi/T_{\rm lin}$ is multiplied by oscillations at a scale of $2\pi/T_{\rm isol}$. These oscillations, although they are associated with nonlinear dynamics and are therefore $\hbar$-dependent, can nevertheless be computed semiclassically without much trouble. One can also readily include recurrences associated with iterates of the time-$T_{\rm isol}$ excursion. This produces a modified envelope, which remains stable until the random oscillations begin at a later time $T_{\rm rand}$ (see Figure 4.)

Because a reloading effect is associated with the isolated homoclinic recurrence as well as with the linear dynamics, the new, modified envelope will multiply the Gaussian random fluctuations arising from long-time dynamics. The final spectrum then has structure on at least three scales. If we take this discrete spectrum and divide through by the linear envelope, we will see fluctuations on top of oscillatory behavior at scale $2\pi/T_{\rm isol}$. If we proceed further to divide out by these identifiable oscillations, we get something that looks like a normal Porter-Thomas spectrum, with no energy-intensity correlations. An example of this situation is described in Section IX, with the numerical results appearing towards the end of Section X.

At this point it may be useful to discuss briefly the relationship between the quantum spectrum and the semiclassical approximation. The initial linear envelope can of course always be obtained semiclassically. The effect of the isolated recurrences can also be computed semiclassically as long as these occur before the breakdown of the semiclassical approximation. The random fluctuations can in principle be computed semiclassically up until the breakdown time, which may be as large as a finite fraction of the Heisenberg time. However, in practice this computation may be difficult for large values of N, because of the exponential proliferation of homoclinic orbits. (This "exponential wall" may be overcome in some systems, making use of the Heisenberg uncertainty principle and of decaying time correlations in the presence of chaos [24].) Eventually, the semiclassical approximation does break down, and the precise locations and intensities of the spectral peaks may differ somewhat between the full quantum mechanics and the semiclassical approximation. There is some ambiguity in the definition of the semiclassical spectrum, due to the non-unitarity of the semiclassical propagator, which has eigenvalues that lie off the unit circle and possesses distinct left and right eigenstates. However, it seems possible to define the spectrum in such a way that the spectral statistics have the properties expected from the discussion above [25]. The *statistical* properties of the quantum spectrum may be very similar to those predicted by the semiclassical approximation, even in the absence of detailed state-to-state agreement.

B. Hamiltonian systems and "quiet time"

In a continuous-time conservative system, like a two-dimensional billiard, another relevant time scale is present in addition to those discussed previously. This scale is δE, the energy width of the initial wavepacket. Clearly, the wavepacket only has a chance to overlap with those eigenstates which lie in the allowed energy range. This can be expressed in terms of an envelope of width δE in the spectrum that all subsequent oscillations have to multiply. In the time domain, this corresponds to the very short-time autocorrelation function, which measures the overlap of the initial wavepacket with itself before it has had a chance to travel a distance comparable with its width. This energy spread scales as $\delta E \sim p\sigma_p = p\hbar/\sigma_q$. For a small wavepacket σ_q, much smaller than the system size L, this scale is well separated from the time of the shortest periodic orbit. This very short time overlap is then followed by a relatively long "quiet period" in which $A(t)$ vanishes. If the original wavepacket lives on a short periodic orbit, eventually a recurrence occurs corresponding to that orbit (and producing an infinite series of bumps under the δE envelope), possibly followed by more quiet time and/or isolated homoclinic recurrences, and eventually random recurrences begin which must be convoluted with all that has come before. In the energy domain, this corresponds to a series of nested envelopes. Of course, the quiet time mentioned above is present even in the absence of scarring, and leads to quantitative predictions about the absence of spectral fluctuations (vanishing of the weighted form factor) on those scales.

VIII. "LINEAR EIGENSTATES" AND OTHER MEASURES OF SCARRING

A. Linear eigenstate scarring

In the preceding sections we have focused on scarring as measured by a Gaussian wavepacket centered on a periodic point. This has led to criteria for scarring such as the distribution of the overlaps of this wavepacket with the eigenstates of the system, the inverse participation ratio, eigenstate-eigenvalue correlations, wavepacket form factors, and the distribution of long-time return probabilities. But we know from previous analysis of the linear approximation

that scarring is associated not only with a periodic point but also with the direction of the classical stable and unstable manifolds near that point. It is reasonable to expect that the hyperbolic nature of the classical dynamics should be seen in the quantum dynamics and in the eigenstates as well. But the Gaussian wavepackets that we have been using so far carry no information even about the linear dynamics around the periodic point.

This serves as motivation for replacing the elliptic wavepacket $\phi_\sigma(q)$ of Eq. 2 with the coherent superposition of Gaussians

$$\phi(q) = Z \int d\beta \; g_{\sigma_\beta}(q) \; e^{-|\beta|/T_0} \, , \tag{28}$$

where $\sigma_\beta = \sigma_0 e^{\lambda\beta}$ and where β is a time parameter, T_0 is a time cutoff, Z is a normalization factor, and $g_\sigma(q)$ is a Gaussian given by Eq. 2. The state ϕ lives on the entire hyperbolic structure surrounding the stable and unstable manifolds, and not only on the fixed point itself. In the limit $T_0 \to \infty$, ϕ is by construction an invariant state of the linearized dynamics around the fixed point. In this sense, ϕ knows about not only the the location of the fixed point, but also about the linear dynamics near that point. The extent to which ϕ differs from being an eigenstate of the full evolution is a measure of the nonlinear dynamics (whereas the extent to which the original Gaussian $g(q)$ differed from being an eigenstate is primarily a measure of the linear instability around the periodic point). The states ϕ are the "linear eigenstates" (they would be true eigenstates if the dynamics were purely linear hyperbolic about the fixed point). We can perform a very similar kind of analysis with ϕ as we did with the plain Gaussians g, in particular looking at the $\langle n|\phi\rangle$ distribution, the inverse participation ratio, the autocorrelation function, and the spectrum. Of course we must choose a value T_0 which is within the linearizable regime of the motion in order to get a sensible result. In this regime, the autocorrelation function for $|T| < T_0$ is given by

$$\begin{aligned} A_\phi(T) &= \langle \phi | U^T | \phi \rangle \\ &= e^{i\theta T} |Z|^2 \int d\tau \frac{1}{\sqrt{\cosh(\lambda\tau)}} \int d\beta \; e^{-|\beta|/T_0} \; e^{-|\beta+\tau-T|/T_0} \, . \end{aligned} \tag{29}$$

We also want T_0 to be large compared to the decay time of the original Gaussian wavepacket, if we are going to see the maximum enhancement of the scarring effect. (The original scarring, as measured for example by the IPR, scales as $T_{\rm decay} \sim 1/\lambda$ for small λ, this being the time for which the linear autocorrelation function is large. The amount of "linear eigenstate" scarring, as measured by overlaps with ϕ rather than g, will scale as T_0, assuming T_0 is large and within the linearizable regime.) So we require

$$1 < \lambda T_0 < \log N = \log \frac{1}{2\pi\hbar} \, , \tag{30}$$

which criterion can be satisfied for small values of $\hbar$. It is important to recognize that the state ϕ is nothing special as far as random eigenstates are concerned, and has the same *a priori* spectral statistics as the states g. From the point of view of the true eigenstates however, the states ϕ are sharp tools which have very large overlaps with specific scarred states. The predicted scar localization scales as T_0, which can be much stronger than the $1/\lambda$ effect detected by g. The state ϕ is much better tuned to the structure of eigenfunctions than is g.

The linear eigenstates idea can be extended to coherent superposition of Gaussians which live on the hyperbolic manifolds just off the periodic orbit. A similar analysis can be made, resulting in the construction of states which in the inverted oscillator analogy correspond to wavefunctions just above or just below the energy of the barrier. We have not carried this out, but it seems likely to be relevant to the hyperbolic states discussed by Nonnenmacher and Voros [17].

Linear eigenstate scarring can be viewed as one of a variety of approximation schemes, where one compares the approximate eigenstates with the eigenstates of the full system and looks for correlations between the two, which indicate that the approximation has some validity. In this sense, the linearized approach, being a log-time approximation, lies between ordinary scarring, which approximates real dynamics only on time scales of order $1/\lambda \approx O(1)$ and a full semiclassical calculation, which can remain valid for times of the order of the Heisenberg time. Unlike the full semiclassical approximation, it has a simple geometrical meaning, being associated with the set of linearized trajectories that come close to, but do not hit, the periodic orbit which is the central object of our analysis.

B. Correlation between periodic points on the same orbit

Given a periodic orbit of a discrete-time map with period $P > 1$, we expect scarred eigenstates to live along the entire orbit and not only at one of the periodic points. In other words, nontrivial correlations should exist in eigenstate

densities measured at different points along a single periodic orbit, so that the entire orbit and not only a section of it is scarred.

More specifically, let us consider a cross-correlation function $A_{ba}(T) = \langle b|U^T|a\rangle$ for wavepackets $|a\rangle$ and $|b\rangle$ centered on two periodic points x_a and x_b. By arguments analogous to those used in Section V, we find that any trajectory taking a homoclinic point on the unstable manifold near x_a to a homoclinic point on the stable manifold near x_b adds coherently with other such trajectories time-shifted along the same homoclinic orbit. The amplification factor resulting from this is again given by the short-time linear return of wavepacket $|a\rangle$ to itself at time $t = nP$ (or equivalently of wavepacket $|b\rangle$ to itself – notice that the short-time autocorrelation functions for the two wavepackets are equal, both coming from the same total instability and phase as accumulated over a traversal of the entire orbit). So we have for the time-averaged probability

$$< |A_{ba}|^2 >_T \; = \sum_n |\langle a|n\rangle|^2 |\langle b|n\rangle|^2 \tag{31}$$

$$\rightarrow \frac{1}{N} \sum_t [\cosh(\lambda t)]^{-1} \, , \tag{32}$$

where λ is the Lyapunov exponent for the period-P orbit. This is to be compared with Eq. 27 obtained previously.

We can also write

$$\begin{aligned} < |A_{ba}|^2 >_T \; &= \sum_n |\langle a|n\rangle|^2 |\langle b|n\rangle|^2 \\ &= < A^*_{bb}(T) A_{aa}(T) >_T \, , \end{aligned} \tag{33}$$

where A_{aa} and A_{bb} are the autocorrelation functions of the two wavepackets. So the result of Eq. 31 can also be thought of as expressing the correlation between the two autocorrelation functions at long times. This is not surprising, given a one-to-one correspondence that can be set up between trajectories leaving and returning to the vicinity of x_a and those that start and end near x_b.

IX. MODEL SYSTEM: GENERALIZED BAKER'S MAPS

As a testing ground for our predictions about nonlinear scarring, we will use the generalized baker's maps, a class of bernoulli systems which are a paradigm of hard chaotic behavior. In addition to having no stable regions of phase space, these systems have the property that the long-time semiclassical dynamics and the semiclassical eigenstates can be computed efficiently (*i.e.* in a time that scales as a power law, rather than exponentially in $1/\hbar$) [24]. This is useful for studying a phenomenon such as scarring, where predictions about the system are made based on our expectations about the statistical properties of the semiclassical behavior. These predictions, obtained in the previous sections, can then be independently compared with the exact semiclassical and the full quantum results, allowing us to distinguish errors in the statistical arguments from errors inherent in the semiclassical approximation itself. As we will see in Section X, semiclassically computed measures of scarring agree only roughly with the results of a full quantum computation for any particular periodic orbit in a given realization of a chaotic quantum system. The fluctuations of the semiclassically computed scarring strengths (when considering an ensemble of orbits with a fixed Lyapunov exponent) are however virtually identical (in mean and variance) to those of the quantum scarring strengths. Any anomalous scarring for a given orbit must be attributed to correlations in new long-time recurrences near the Heisenberg time, such correlations being present in both the semiclassical and full quantum computations.

We will discuss briefly the definition and properties of the classical, semiclassical, and quantum generalized baker's map, referring the reader to the literature on the subject for more details [26,27]. Classically, the map is defined as a map of the unit square onto itself, where the square is initially cut up into M vertical strips with widths w_m ($\sum_{m=0}^{M-1} w_m = 1$) and height 1. (In the original baker's map, $M = 2$ and the two strips each have width 1/2. This leads to a constant Lyapunov exponent of $\log(2)$ everywhere in phase space. In the generalized version of these maps, this restriction is lifted, allowing different periodic orbits of the same length to have different instability factors.) Each strip is stretched horizontally and compressed vertically, in an area-preserving way, so that the width becomes 1 and the height becomes w_m. The deformed horizontal strips are finally stacked on top of each other, in some order (conventionally, the left-to-right order of the initial arrangement corresponds to the bottom-to-top order of the final one). If we define $s_m = \sum_{j<m} w_j$ to be the left edge of the m-th strip, we have

$$\begin{aligned} x' &= (x - s_m)/w_m \\ p' &= w_m p + s_m \end{aligned} \tag{34}$$

for x in the m-th strip, $s_m \le x < s_{m+1}$. Trajectories and periodic orbits can be labeled symbolically by strings of digits, each between 0 and $M-1$, the T-th digit indicating the horizontal strip in which the particle is found at time T. A simple nontrivial example is the $\ldots 11111 \ldots$ orbit for the case $M = 3$. The instability exponent of this orbit is given by $|\log(w_1)|$, and homoclinic orbits of various instabilities and phases can be constructed (*e.g.* $\ldots 111112001202011111 \ldots$). This is in fact the periodic orbit that we will use for the numerical data on scarring in Section X.

A quantum mechanical version of this system can be obtained readily for any value of Planck's constant given by $h = 1/N$. N is the dimension of the resulting Hilbert space. The position basis consists of states $|j\rangle$, $j = 0 \ldots N-1$, corresponding semiclassically to vertical strips located at $x_j = (j + \epsilon_1)/N$. Similarly, the momentum basis is formed by $|\tilde{k}\rangle$, $\tilde{k} = 0 \ldots N-1$, with the states living at $p_{\tilde{k}} = (\tilde{k} + \epsilon_2)/N$. The two bases are related by a discrete fourier transform. The numbers $\epsilon_{1,2} \in [0, 1)$ are constants which provide the quantization conditions for the system (they define the phases associated with going around the torus in the vertical and horizontal directions, respectively).

To define the baker's map dynamics we write N as a sum of integers $N = \sum_{m=0}^{M-1} N_m$, approximating the classical division of phase space into strips ($|N_m - w_m N| < 1$). Then the leftmost N_0 position states are mapped into the bottom N_0 momentum states by a discrete fourier transform, and similarly for each of the other strips. Finally, we transform back to the position basis. So the one-step evolution operator in the position basis has the form

$$U = \left[F_N^{-1}\right] \begin{bmatrix} e^{i\theta_0} F_{N_0} & 0 & \ldots & 0 \\ 0 & e^{i\theta_1} F_{N_1} & \ldots & 0 \\ \vdots & \vdots & \ddots & \vdots \\ 0 & 0 & \ldots & e^{i\theta_{M-1}} F_{N_{M-1}} \end{bmatrix}, \tag{35}$$

where F_N is a discrete fourier transform matrix on N sites, and the θ_m are arbitrary angles. Different choices of θ_m correspond to different semiclassical theories, all having the same classical limit. The statistical properties of the quantum mechanical system should be independent of the choice of quantization parameters $\epsilon_{1,2}$ and θ_m, so these can be randomly chosen in the context of an ensemble averaging.

The semiclassical one-step propagator can be easily written down in the position basis in terms of the stretching factors w_m and phases θ_m, making use of the symbolic dynamics governing this system.

$$U_{\mathrm{SC}}(x', x) = \sum_m \sqrt{w_m} e^{i s_m x'/\hbar + i\theta_m} \delta(x - (s_m + w_m x')) \,. \tag{36}$$

The exact semiclassical $T-$step propagator is obtained by iterating the one-step formula T times (this is permitted as long as we do not impose the quantization condition by forcing x at intermediate times to have one of the N quantum mechanically allowed values). Long-time overlaps of Gaussian wavepackets, as well as semiclassical spectra and eigenstates can be computed in an efficient manner (for example, by fourier transforming to momentum variables and cutting off the high-frequency modes) [24]. These calculations generally show good agreement with the quantum results, although the convergence is not uniform over phase space [25]. In particular, the semiclassical approximation does not see the "diffractive" effects associated with the boundaries between classical strips.

To illustrate the effect of isolated returning orbits as discussed in Section VII A, we construct a modified version of the system described above. A rectangle is divided into $2L+1$ strips numbered $-L \ldots +L$. The strips $-L \ldots -1$ all have the same width, and similarly for strips numbered $+1 \ldots +L$. Now the three vertical strips $-L$, 0, and $+L$ get mapped into the horizontal region spanned by strips -1, 0, and $+1$, via the usual generalized baker's map dynamics for $M = 3$ described in the above paragraphs. Simultaneously strip i for $1 < i < L-1$ gets shifted to the right into strip $i+1$, and similarly $-i$ is shifted to the left into $-(i+1)$. In effect, we have two long corridors to the left and right of the hyperbolic region, each of which must be traversed in its entirety before one returns to the center, which is where all of the mixing occurs. This slows down the total mixing in phase space because each excursion away from strip 0 takes at least L steps. An effective symbolic dynamics using the three symbols '0', '$-$', and '+' can be used to represent the trajectories, where '+'$= +1 + 2 \ldots + L$, and similarly for '$-$'. Then for the periodic orbit $\ldots 0000 \ldots$, the shortest homoclinic excursions involve L steps, and are symbolically represented as $\ldots 000 + 000 \ldots$ and $\ldots 000 - 000 \ldots$. On the other hand, the Lyapunov exponent of the original orbit (and therefore the decay time of the linear dynamics) can be arranged to be of order unity, creating a clean separation of scales between the two effects. Numerical results for this system will be presented towards the end of Section X.

X. NUMERICAL RESULTS

We now proceed to examine the numerical evidence for scarring in the three-strip generalized baker's map described in the previous section. We concentrate on the period one orbit $\ldots 11111 \ldots$, for which the particle stays always in

the middle strip. The location of the fixed point is given by $x_{\rm FP} = p_{\rm FP} = w_0/(w_0 + w_2)$, and the Lyapunov exponent is $\lambda = |\log w_1|$. An ensemble average can be performed over different strip widths w_0, w_1, and w_2, and over the value of Planck's constant $\hbar = 1/2\pi N$. The integers N_m, describing the dimensions of the subspaces corresponding to the three strips, are chosen to be prime to eliminate possible sources of anomalous behavior. (In the original baker's map, such anomalous behavior is associated with values of N which are divisible by powers of 2; see for example Ref. [24].) Also, we demand $N_0 \neq N_2$ to eliminate the parity symmetry. This parity symmetry, also present in the original baker's map and given by $P : x \to 1-x,\ p \to 1-p$, would otherwise produce a factor of 2 enhancement in the inverse participation ratio for the $\ldots 11111 \ldots$ orbit, as explained in the concluding paragraph of Section VI D.

For each of 97 realizations of this system, the inverse participation ratio was computed for a circular wavepacket centered on the periodic point. The Lyapunov exponent for the orbit ranged from a low value of 0.28 (corresponding to a linear IPR enhancement factor of 10.4 according to Eq. 27, and not including the quantum fluctuation factor F), to a high value of 1.94, corresponding to a linear prediction of 1.66 for the IPR. The values of N in this ensemble lie between 129 and 419. In Figure 5, the actual quantum value of the IPR is plotted (using squares) *versus* the linear prediction on the horizontal axis. The data is compared to a line of slope 2.2, corresponding to the quantum fluctuation factor F appropriate to this system. F is obtained here by measuring the mean IPR for a wavepacket placed randomly in the phase space instead of on a periodic point. We see large fluctuations in this Figure around the predicted behavior, but the overall linear trend is certainly correct. Fluctuations in the amount of scarring at a given value of the Lyapunov exponent are of the order of twenty percent around the mean. This level of variation in scarring strength from orbit to orbit is quite reasonable taking into account the fact that the effective number of spectral lines under the linear envelope is well under 100 in most cases studied. (This effective dimension of the space in which the wavepacket lives is given by the total dimension N divided by the IPR of the linear envelope.)

For a subset of 46 out of this set of 97 systems, the semiclassical IPR was also computed (this is defined by the fluctuation of the *right* eigenstates of the time evolution). These values are shown on the same plot in Figure 5 using the '+' symbol. The semiclassical IPR is correlated with but does not exactly follow the full quantum value. Deviations from the predictions of the random statistical theory are present in the semiclassical as well as in the quantum calculation. This suggests that cases of excessive (or deficient) scarring must be associated with non-randomness in the new long-time recurrences, and not simply with a breakdown of the semiclassical approximation. Given the small number of parameters defining the system, and the finite dimension N of the Hilbert space, such occasional anomalous behavior is not very surprising.

On the same Figure, we also plot (using triangles) the results for a modified version of the generic baker's map, where random matrices have been substituted for the matrices F_{N_0} and F_{N_2} describing the dynamics of the left and right strips (while leaving the behavior of the middle strip unchanged). This corresponds to explicitly randomizing the long-time recurrences, while preserving the constraint imposed by the short-time dynamics in the region of the fixed point. The full IPR in this case follows the same linear dependence on the short-time envelope prediction, but with a clearly smaller numerical coefficient F. This is consistent with the finding that the generic wavepacket-averaged (non-scarred) value of the IPR for this system is smaller (2.0 compared with 2.2 for the true baker's map).

In Figure 6, the ratio between the actual IPR and the linearly predicted value is plotted (squares) as a function of the effective system size $N_{\rm eff} = N/{\rm IPR}_{\rm lin}$. We find significant fluctuations around the mean value of 2.5, with no evident trend as $N_{\rm eff}$ increases. In a random matrix theory model, fluctuations around the mean value of the IPR scale as $1/\sqrt{N_{\rm eff}}$, and this behavior is not inconsistent with the data, although the range of N used is not sufficient to see the convergence. On the same Figure, the corresponding ratio is plotted (using triangles) for the "randomized baker's map" described in the previous paragraph. Here the fluctuations around the mean are only slightly smaller than for the real baker's map (their magnitude being about 15 rather than 20 percent). The mean value of the full-to-linear-IPR ratio is also smaller, as explained in the previous paragraph. For the explicitly randomized system, the only correlations in the new long-time recurrences (after having taken into account the short-time constraint) are due to the finiteness of the Hilbert space, and are expected to become insignificant in the $\hbar \to \infty$ limit.

So far we have been focusing on the second moment of the spectral intensity distribution, for various realizations of the generalized baker's map system. We now turn to a specific system, for which we will be able to look at the entire spectrum and see explicitly the pattern of fluctuations around the linear envelope. We choose the first entry in our data file, with $N = 223$ and three strips of widths $N_0 = 79$, $N_1 = 101$, and $N_2 = 43$. The Lyapunov exponent for the $\ldots 11111 \ldots$ orbit is 0.79, producing by Eq. 27 a linear envelope with an IPR of 3.97. The actual quantum value of the IPR is 7.93, so there is a Heisenberg-time fluctuation factor of 2.0 (compared to the expected value 2.2). The semiclassically computed value for the IPR is somewhat larger, at 8.46.

The intensity spectrum for a circular wavepacket centered on the fixed point is plotted in Figure 7a, along with the linear envelope $S_{\rm lin}(E)$ and an intermediate envelope obtained by fourier transforming $A(T)$ for $|T| < 30$. The intermediate envelope corresponds to a time scale large compared to the linear decay time and mixing time of the system, but still small compared with the Heisenberg time. A semiclassical version of this intermediate envelope is also plotted and is seen to be very similar to the full quantum computation. In Figure 7, a portion of the line spectrum is

compared with the same spectrum computed semiclassically. (Again, the semiclassical spectrum is defined by taking the overlaps between the wavepacket and the right eigenstates of the semiclassical evolution. The imaginary parts of the semiclassical energies are ignored.) In Figure 7c, the quantum spectrum of Figure 7a is now plotted after dividing out by the linear envelope. We see that the underlying oscillations around the envelope are in fact energy independent, and are equally strong near the peak and valley of the envelope.

In Figure 8, a histogram of these scaled intensities is plotted, after averaging over several realizations of the system. This is compared to a similar histogram of the unscaled intensities. It is seen that the former comes much closer to obeying an exponential law as predicted by Porter-Thomas.

In Figure 9, the spectral correlation function $< S(\epsilon + E)S(\epsilon) > / < S(\epsilon) >^2$ is plotted in the form of a histogram (plusses), and compared to the correlation function for a scaled spectrum (diamonds). An ensemble average and an average over the energy ϵ has been performed in each case. We can see that the correlation function for the scaled spectrum is uniform with small random fluctuations (we ignore the large correlations for E of the order of a mean level spacing, $E = O(1/N)$). On the other hand, correlations in the unscaled spectrum are very striking, and sharply peaked near $E = 0$.

In Figure 10, a spectrum with a linear and a second-order envelope is plotted for a system with isolated homoclinic recurrences, associated with excursions away from the mixing region as discussed at the end Section IX. We choose a minimum excursion length $L = 23$, with strip 0 having width $N_0 = 17$ and all the others being of width $N_{\pm 1} = \ldots = N_{\pm 23} = 19$. A gaussian wavepacket is launched at the center of the middle strip. The initial linear decay occurs within 1 – 2 time steps (the Lyapunov exponent at the fixed point being 1.17), but the initial recurrence, corresponding to the homoclinic orbit $\ldots 0000 + 0000 \ldots$ and its parity counterpart $\ldots 0000 - 0000 \ldots$ does not peak until $T = 28$. The next set of recurrences results from the classical orbits $\ldots 0000 + 0^n + 0000 \ldots$ and $\ldots 0000 + 0^n - 0000 \ldots$, and their parity counterparts (n being a nonnegative integer). In all, 12 identifiable peaks with spacing ~ 23 can be identified, the structure not breaking down completely until $T \sim 300$, at which time random mixing begins to take over (classically, homoclinic excursions with more and more insertions of the '0' symbol are becoming important here for entropic reasons). The squared autocorrelation function for the wavepacket is plotted in Figure 10.

In Figure 11, the corresponding energy spectrum is plotted along with a linear envelope (dotted line) and an envelope resulting from the first two sets of recurrences (up to two insertions of '+' or '−'), dashed line. The solid curve includes the effects of the first six sets of homoclinic returns.

XI. CONCLUSION

By focusing on the importance of nonlinear recurrences, long-time fluctuations, symmetry factors, and the local classical structure around a periodic orbit, we have attempted to clear up some of the long-standing mysteries in the literature on scarring. We have seen that the linear theory, even in a worst-case "egalitarian" scenario, makes a lower bound prediction on scarring strength that is a function of the instability of the orbit only, and independent of energy and $\hbar$. Generically, we expect random long-time fluctuations to be present, associated with nonlinear excursions away from the periodic orbit. When these gaussian random fluctuations are included in the theory, quantitative agreement between theory and numerics is obtained using measures such as the inverse participation ratio, wavefunction intensity distribution, and correlations in the local density of states. Scarring stronger than that predicted by the random nonlinear theory can be obtained in the presence of identifiable homoclinic recurrences.

The formalism developed here lends itself naturally to the investigation of other effects of short-time dynamics on the properties of quantum eigenstates. Such short-time behavior may involve classical structures other than periodic orbits, diffraction, and "quiet time" behavior. Intensity correlations among eigenstates as well as phase space correlations in the structure of individual eigenstates can be studied. Interesting questions arise in the design of "optimal" measures for observing this class of deviations from random matrix theory behavior.

The nonlinear scarring theory as presented in this paper has been used recently to study the tail of the wavefunction intensity distribution in chaotic systems [29]. Predictions, validated by numerical experiments, have been obtained for the distribution of eigenstate intensities in a single region of phase space, for phase space-averaged distributions, and also for ensembles which include systems with orbits of different lengths and instability exponents. Power-law tails are naturally obtained in the process of ensemble averaging, under certain assumptions.

XII. ACKNOWLEDGMENTS

This research was supported by the National Science Foundation under grant number CHE-9321260. We wish to thank the Institute for Theoretical Physics at UCSB, where this research was initiated, for its hospitality. We also

wish to thank the Isaac Newton Institute for the Mathematical Sciences in Cambridge, where this work was completed. EJH would like to thank S. Tomsovic for many stimulating conversations.

---

[1] M. V. Berry, in *Chaotic Behaviour of Deterministic Systems*, ed. by G. Iooss, R. Helleman, and R. Stora (North-Holland 1983) p. 171.
[2] O. Bohigas, M.-J. Giannoni, and C. Schmit, *J. Physique Lett.* **45**, L-1015 (1984).
[3] E. J. Heller, *Phys. Rev. Lett.* **53**, 1515 (1984).
[4] S. Tomsovic and E. J. Heller, *Phys. Rev. Lett.* **70**, 1405 (1993); S. Tomsovic and E. J. Heller, *Phys. Rev.* **E 47**, 282 (1993).
[5] P. O'Connor, J.N. Gehlen, and E.J. Heller, *Phys. Rev. Lett.* **58**, 1296 (1987).
[6] S. Sridhar, *Phys. Rev. Lett* **67**, 785 (1991).
[7] J. Stein and H.-J. Stöckman, *Phys. Rev. Lett.* **68**, 2867 (1992).
[8] T. M. Fromhold, P. B. Wilkinson, F. W. Sheard, L. Eaves, J. Miao, and G. Edwards, *Phys. Rev. Lett.* **75**, 1142 (1995); P. B. Wilkinson, T. M. Fromhold, L. Eaves, F. W. Sheard, N. Miura, and T. Takamasu, *Nature* **380**, 608 (1996).
[9] D. Wintgen and A. Honig, *Phys. Rev. Lett.* **63**, 1467 (1989).
[10] K. Muller and D. Wintgen, *J. Phys.* **B 27**, 2693 (1994).
[11] E. B. Bogomolny, *Physica* **D 31**, 169 (1988).
[12] M. V. Berry, Les Houches Lecture Notes, Summer School on Chaos and Quantum Physics, M-J. Giannoni, A. Voros, and J. Zinn-Justin, eds., Elsevier Science Publishers B.V. (1991); M.V. Berry, *Proc. Roy. Soc.* **A 243**, 219 (1989).
[13] R. Aurich and F. Steiner, *Chaos, Solitons and Fractals* **5**, 229 (1995).
[14] O. Agam and N. Brenner, *J. Phys.* **A 28**, 1345 (1995).
[15] O. Agam and S. Fishman, *Phys. Rev. Lett.* **73**, 806 (1994); O. Agam and S. Fishman, *J. Phys.* **A 26**, 2113 (1993).
[16] S. Fishman, B. Georgeot, and R. E. Prange, *J. Phys.* **A 29**, 919 (1996).
[17] S. Nonnenmacher and A. Voros, *J. Phys.* **A 30**, 295 (1997).
[18] M. V. Berry and M. Tabor, *Proc. Roy. Soc.* **A 349**, 101 (1976); M. V. Berry and M. Tabor, *J. Phys.* **A 10**, 371 (1977).
[19] P. W. O'Connor and E. J. Heller, *Phys. Rev. Lett.* **61**, 2288 (1988).
[20] A. I. Schnirelman, *Usp. Mat. Nauk.* **29**, 181 (1974); Y. Colin de Verdiere, *Commun. Math. Phys.* **102**, 497 (1985); S. Zelditch, *Duke Math. J.* **55**, 919 (1987).
[21] E. J. Heller, Wavepacket Dynamics and Quantum Chaology in *Chaos and Quantum Physics*, Eds. M. J. Giannoni, A. Voros, and J. Zinn-Justin, Elsevier Science Publishers, Amsterdam (1990).
[22] B. Li, *Phys. Rev.* **E 55**, 5376 (1997).
[23] L. Kaplan and E. J. Heller, Weak Quantum Ergodicity, *Physica* **D**, in press.
[24] L. Kaplan and E. J. Heller, *Phys. Rev. Lett.* **76**, 1453 (1996); F.-M. Dittes, E. Doron, and U. Smilansky, *Phys. Rev.* **E 49**, R963 (1994).
[25] L. Kaplan and E. J. Heller, unpublished.
[26] N. L. Balazs and A. Voros, *Europhys. Lett.* **4**, 1089 (1987); N. L. Balazs and A. Voros, *Ann. Phys. (N. Y.)* **190**, 1 (1989); M. Saraceno, *Ann. Phys. (N. Y.)* **199**, 37 (1990); M. Saraceno and A. Voros, *Physica* **D 79**, 206 (1994).
[27] P. W. O'Connor, S. Tomsovic and E. J. Heller, *Physica D* **55**, 340 (1992); P. W. O'Connor and S. Tomsovic, *Ann. Phys. (N. Y.)* **207**, 218 (1991).
[28] E. J. Heller, *J. Chem. Phys.* **72**, 1337 (1980); E. J. Heller and M. J. Davis, *J. Phys. Chem.* **86**, 2118 (1982); E. B. Stechel and E. J. Heller, *Ann. Rev. Phys. Chem.* **35**, 563 (1984); E. J. Heller, *Phys. Rev.* **A35**, 1360 (1987).
[29] L. Kaplan, unpublished.

FIG. 1. The short time dynamics of the localized wavepacket imposes an envelope in the local density of states which the resolved spectrum (coming from long-time dynamics up to times of order of the Heisenberg time) must obey. The envelope has a peak at quasi-energy $\epsilon = \theta$, a width $\delta\epsilon \sim \mathcal{O}(\lambda)$, and a height $\sim \mathcal{O}(1/\lambda)$.

FIG. 2. The short time dynamics by itself does not predict whether "totalitarian" (top) or "egalitarian" (bottom) filling of the local density of states envelope occurs. Both spectra have the same short time local density of states envelope.

FIG. 3. Nonlinear recurrences resulting from following a homoclinic classical orbit. Linear wavepacket spreading is followed by a nonlinear excursion, and finally by an approach back to the fixed point along the stable manifold. Three levels of abstraction are shown. Diagram A shows a portion of the stable manifold, and a longer portion of the unstable manifold. B is more schematic, showing how a small rectangle in the initial disk (representing the initial state in phase space) is compressed and stretched, finally returning along the stable manifold. Note that this particular rectangle is special in that it returns soon, guided by a primary homoclinic trajectory. In C, we see a regularized (normal form) version of B. Two types of correlation are seen in this Figure. In B, for example, "1" and "5" have exactly the same phase relation as "2" and "6". Also "5" and "6" are related by a phase associated with one iteration of the periodic orbit.

FIG. 4. A strong, isolated recurrence at a time later than the Lyapunov decay time causes additional structure in the spectrum at a higher resolution. This new, oscillating envelope further constrains the possible behavior of the resolved spectrum. The final spectrum has structure on at least three scales.

FIG. 5. A plot of the actual value of the inverse participation ratio (IPR) for a wavepacket centered on a periodic orbit (squares), *versus* the value predicted by the linear theory. IPR's in the semiclassical approximation are plotted using the '+' symbol, and IPR's in a baker's map with random matrix theory nonlinear behavior are plotted with triangles.

FIG. 6. Here the ratio of the full IPR to the value predicted by the linear theory is plotted against the effective number of states that the wavepacket can overlap with (according to the linear theory). Using triangles, the same quantity is plotted for a randomized baker's map.

FIG. 7. In (a), the full spectrum is plotted along with the linear envelope (dotted line), an intermediate envelope corresponding to $|T| < 30$ (solid line), and a semiclassical intermediate envelope (dashed line). In (b), a portion of the spectrum (solid) is compared to the spectrum obtained using semiclassical eigenstates (dashed). In (c), the quantum spectrum has been divided out by the linear envelope of (a).

FIG. 8. A histogram of scaled spectral intensities (diamonds) after having divided out by the linear envelope, compared to a histogram of raw (unscaled) intensities (plusses). The Porter-Thomas exponential law is plotted as a solid line. All distributions are defined to have a mean value of one.

FIG. 9. The two-point spectral correlation function of the scaled spectrum (diamonds) is compared to the correlation function of the raw spectrum (plusses), after ensemble and energy averaging.

FIG. 10. The quantum return probability as a function of time for the modified baker's map with a minimum excursion length of $L = 23$.

FIG. 11. The spectrum corresponding to the wavepacket whose return probability is plotted in the previous Figure, along with a linear envelope (dotted line), an intermediate envelope corresponding to the first two sets of homoclinic recurrences (dashed line), and higher resolution envelope corresponding to the first six sets of recurrences (solid line).

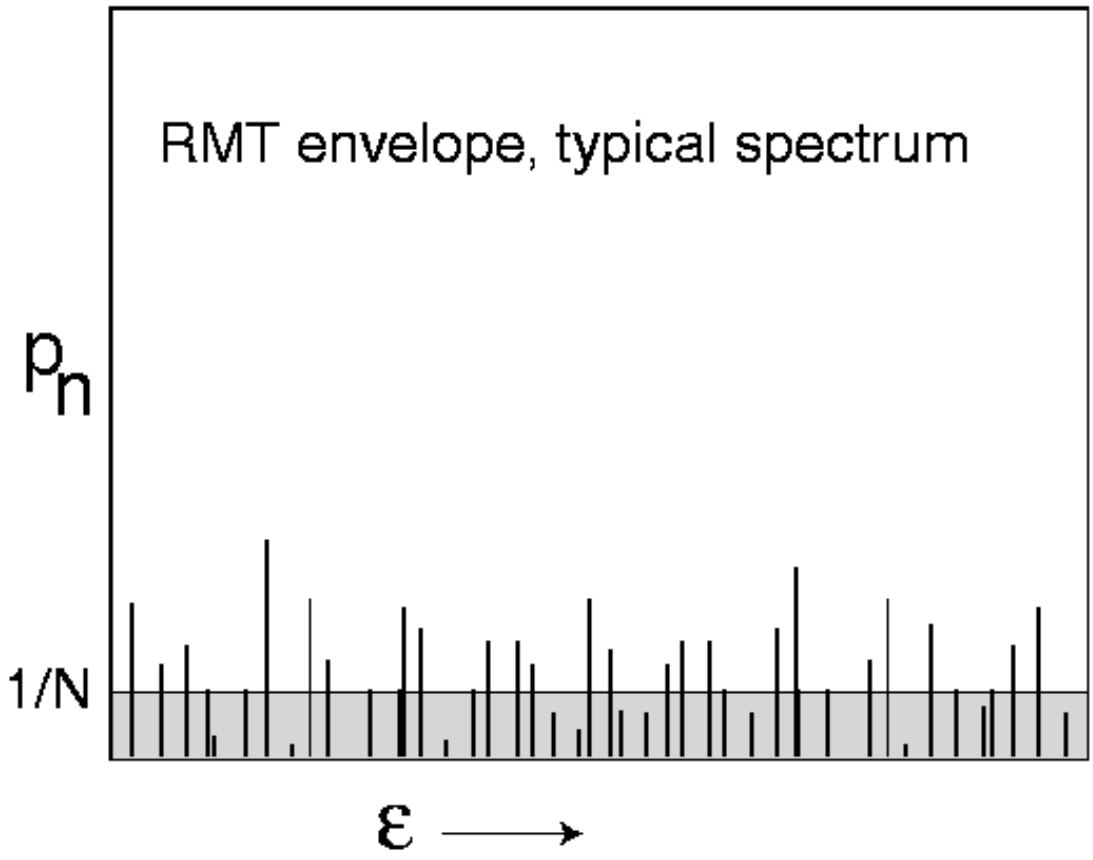
RMT envelope, typical spectrum
p_n
1/N
$\varepsilon \longrightarrow$

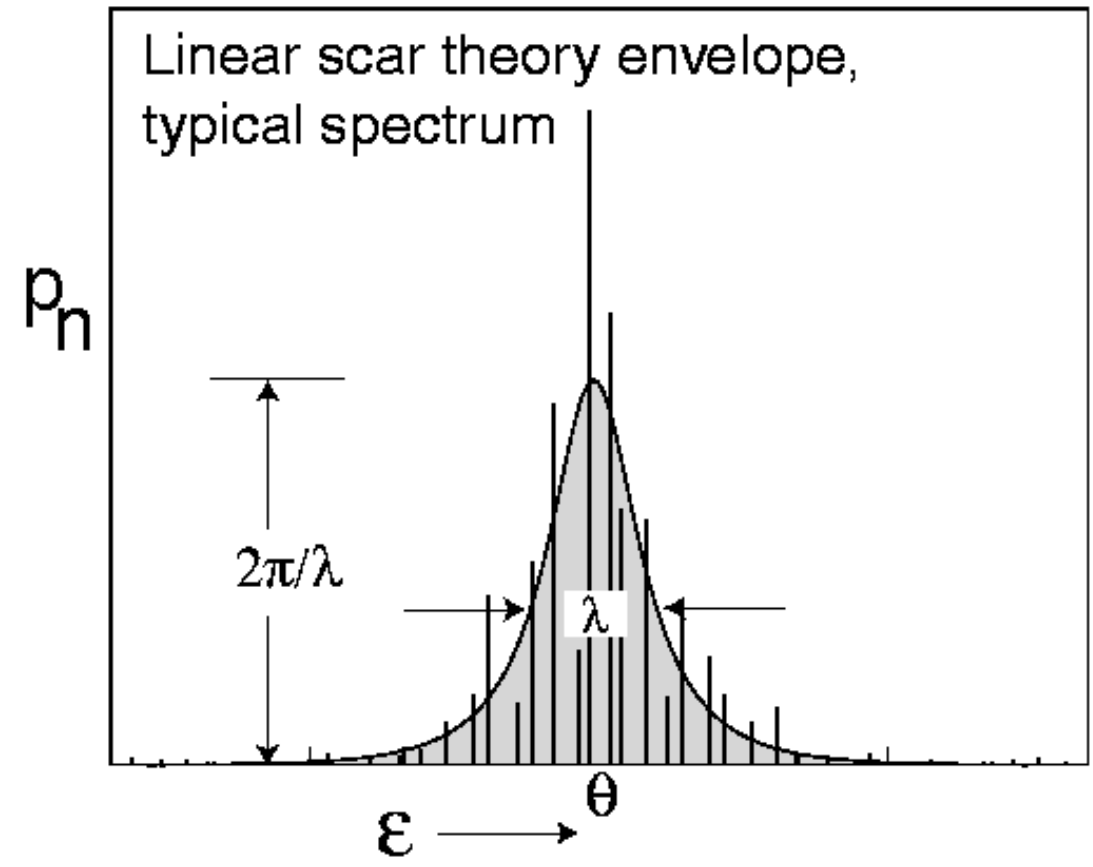
Linear scar theory envelope,
typical spectrum
p_n
$2\pi/\lambda$
λ
θ
$\varepsilon \longrightarrow$

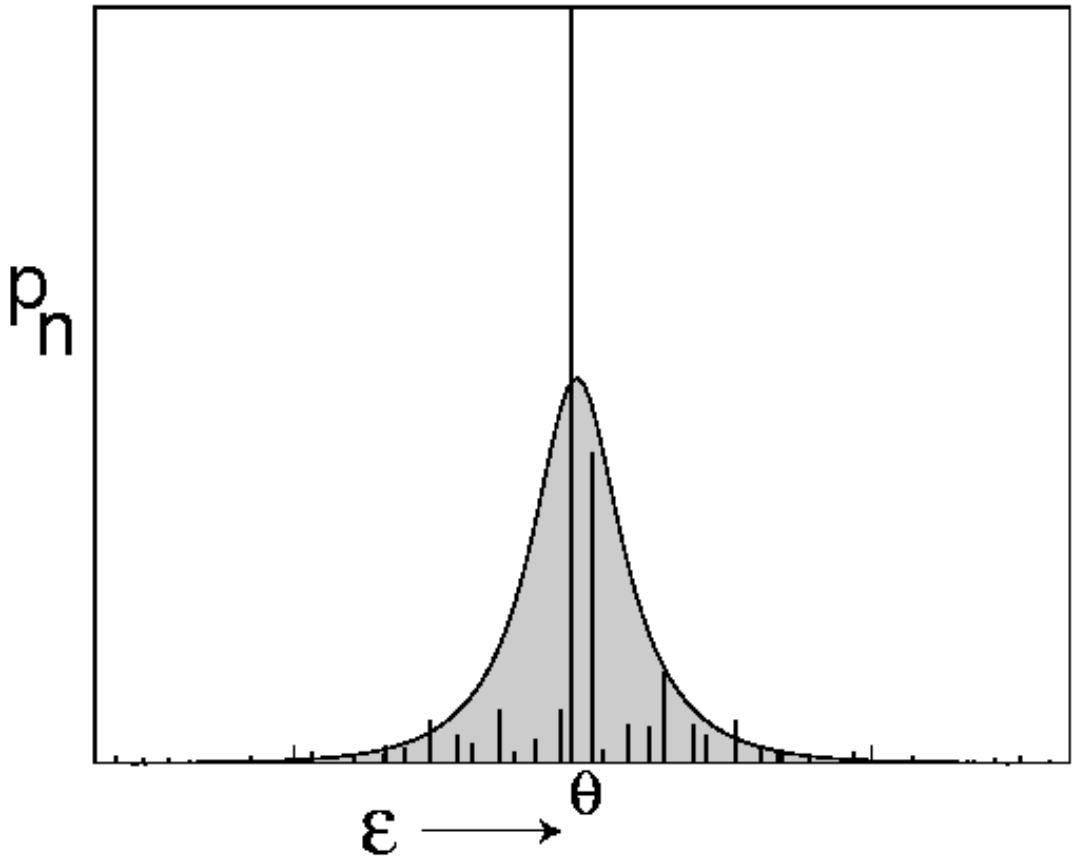
p_n
θ
ε

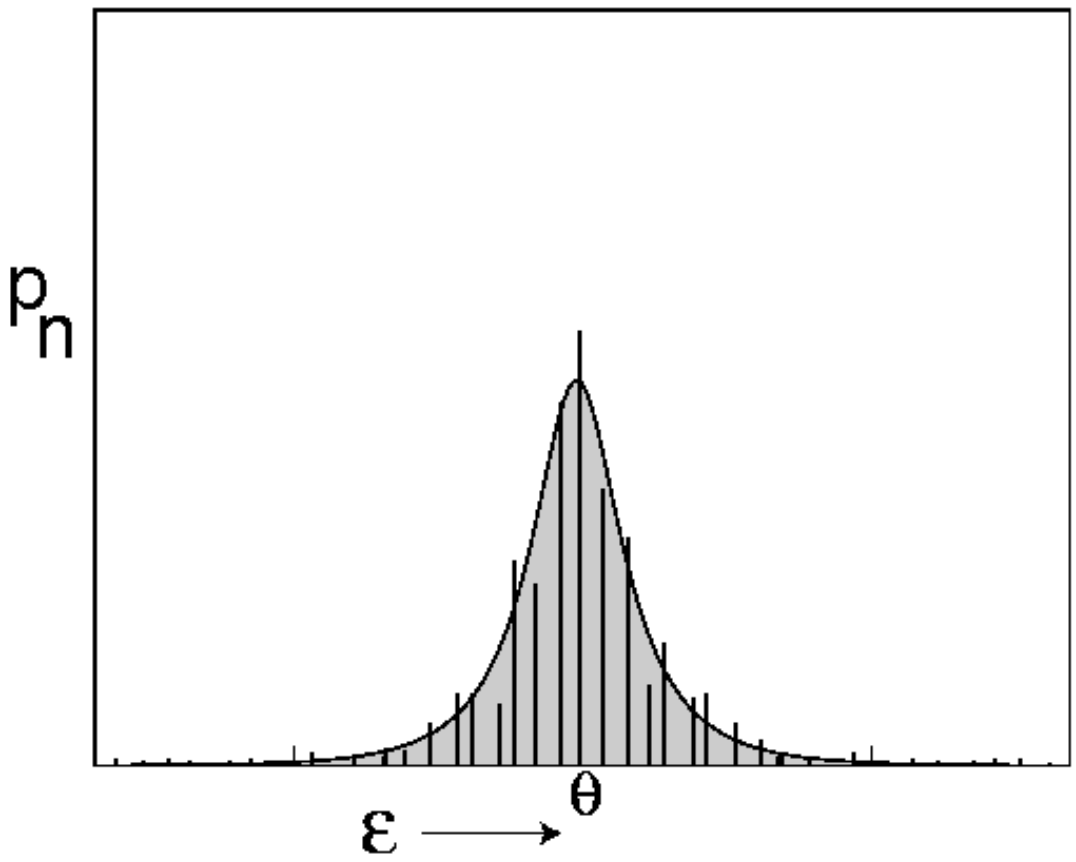
p_n
θ
ε

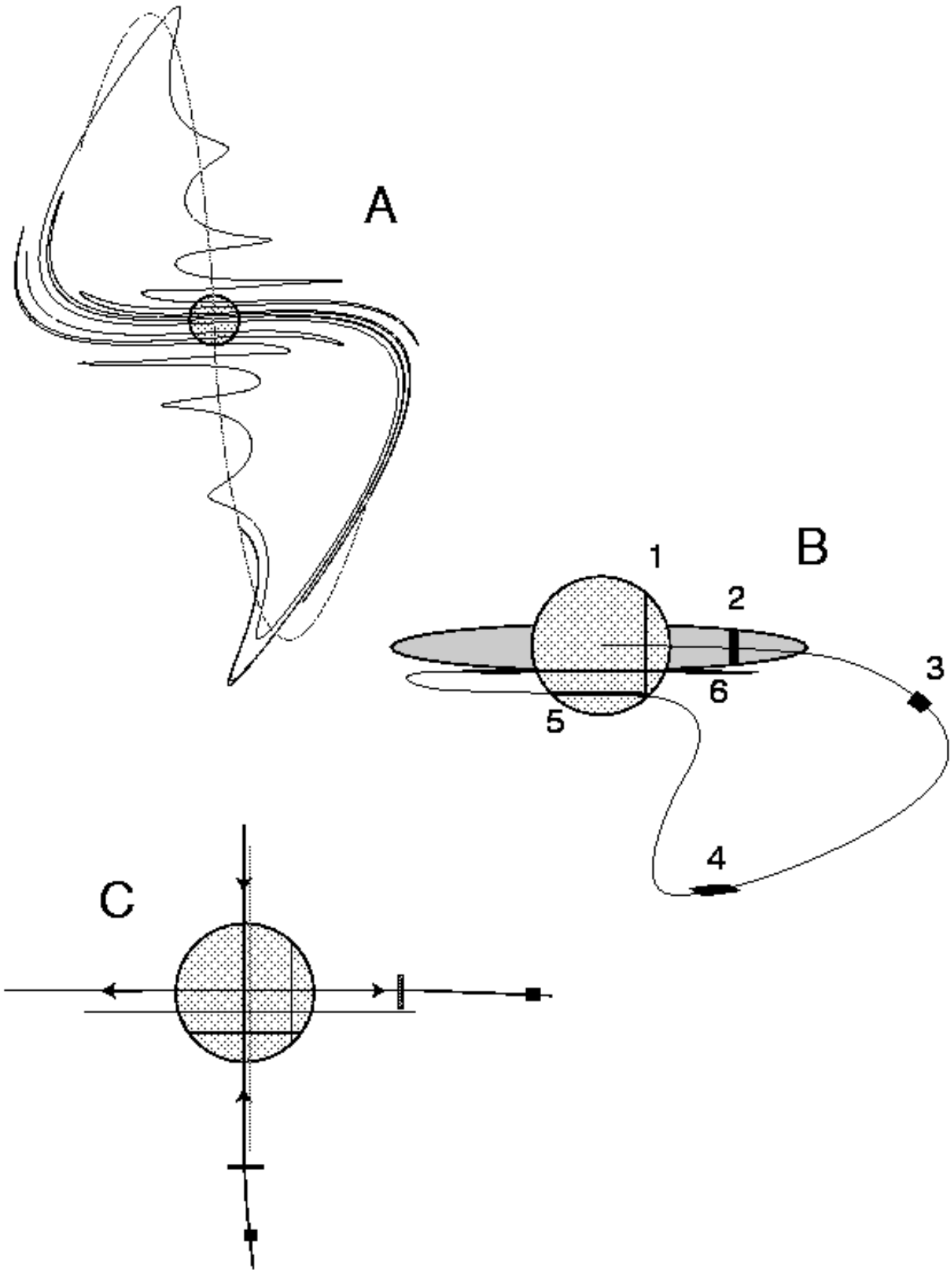
A
B
1
2
3
4
5
6
C

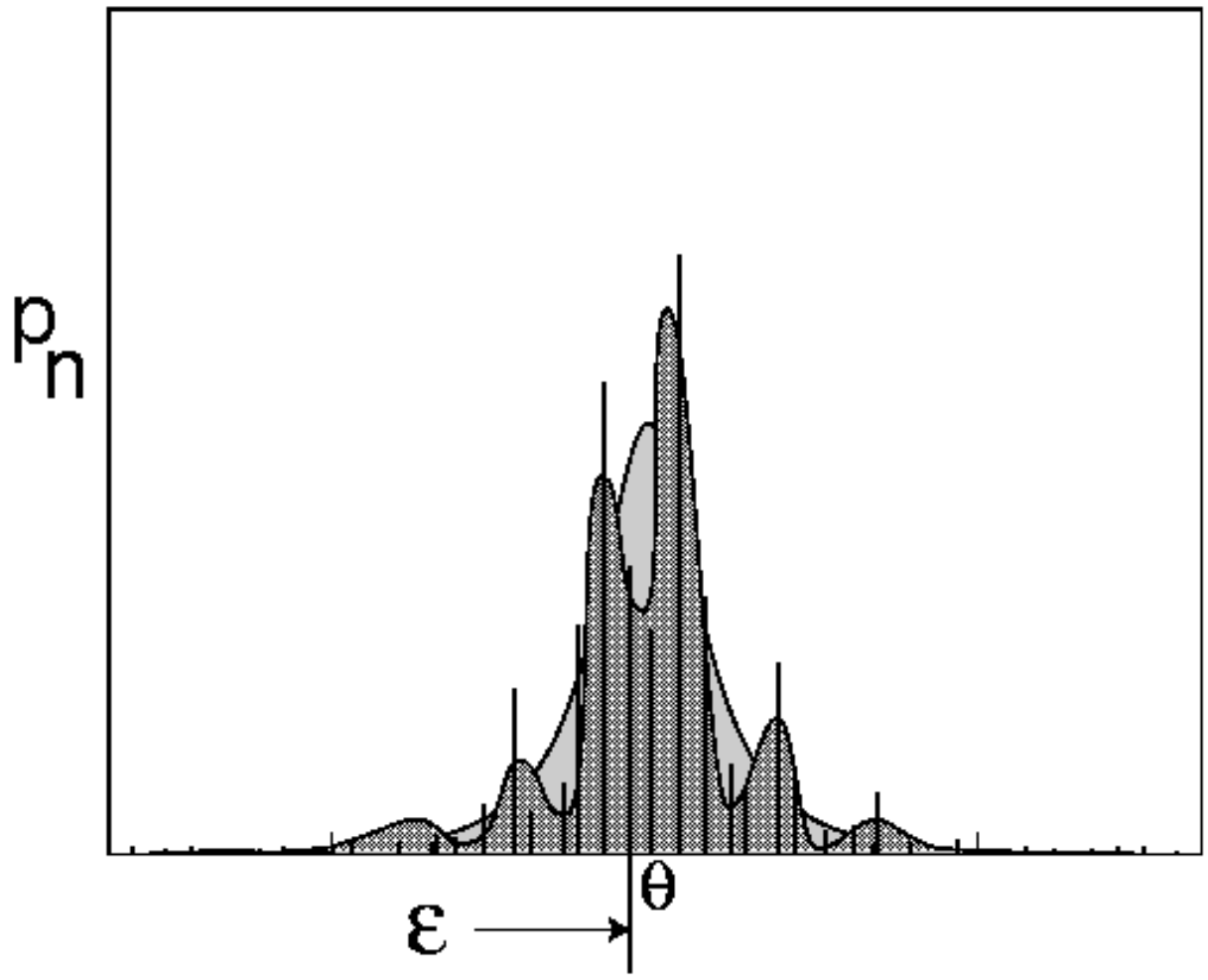
p_n
θ
ε

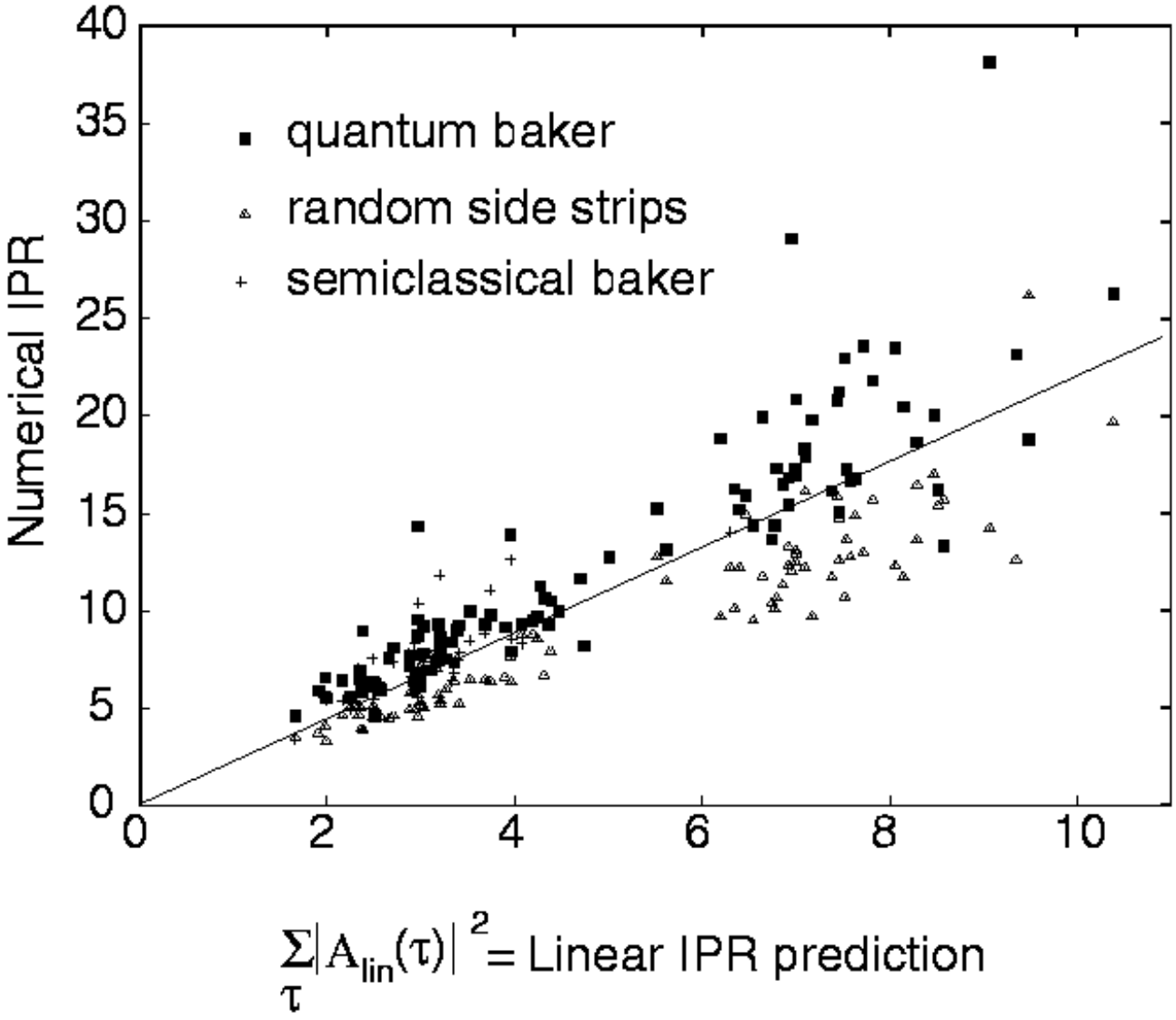
quantum baker
random side strips
semiclassical baker
Numerical IPR
$\sum_{\tau} |A_{lin}(\tau)|^2$ = Linear IPR prediction
0
5
10
15
20
25
30
35
40
0
2
4
6
8
10

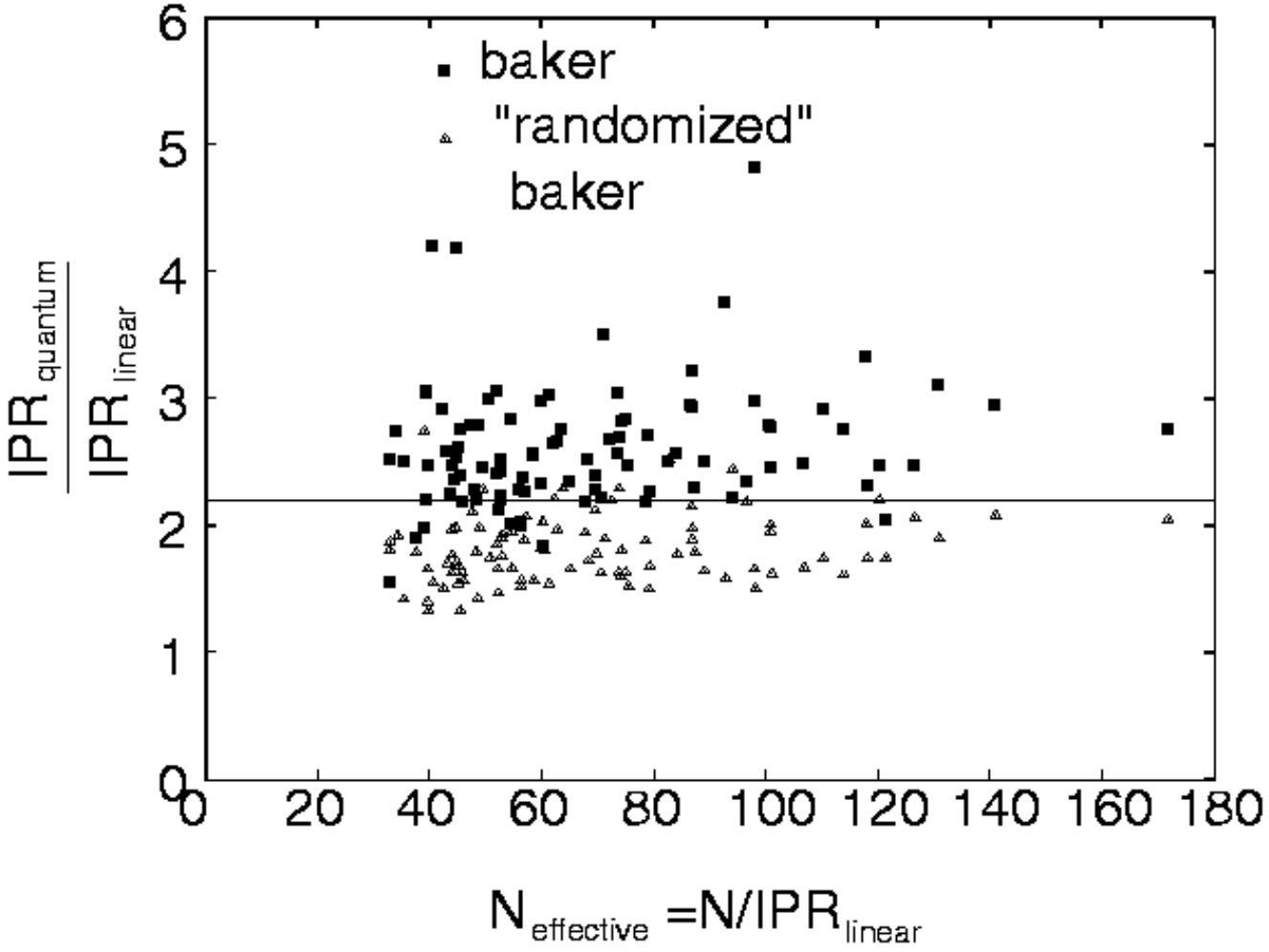
baker
"randomized"
baker
$\frac{IPR_{quantum}}{IPR_{linear}}$
$N_{effective} = N/IPR_{linear}$
0
1
2
3
4
5
6
0
20
40
60
80
100
120
140
160
180

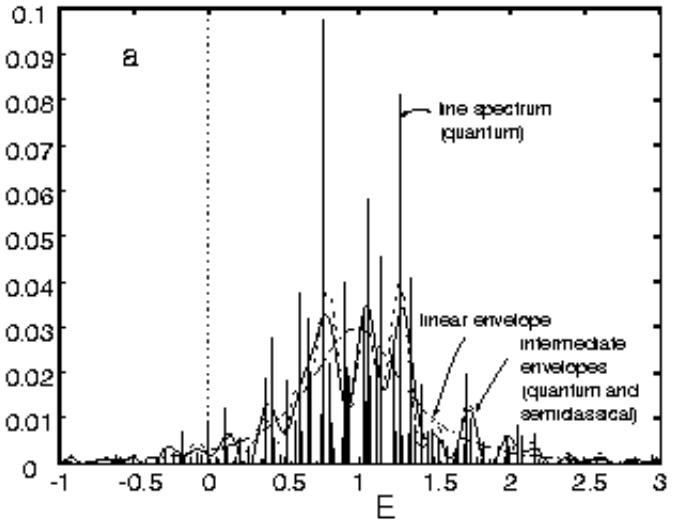
a
line spectrum
(quantum)
linear envelope
intermediate
envelopes
(quantum and
semidassical)
E

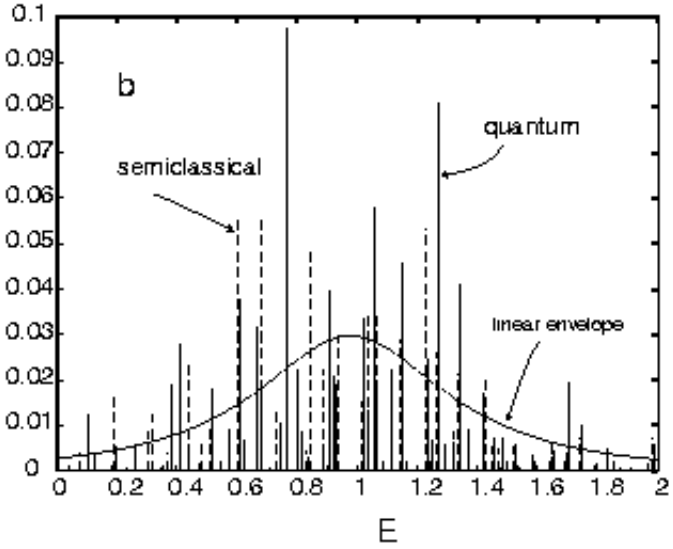
b
quantum
semiclassical
linear envelope
E

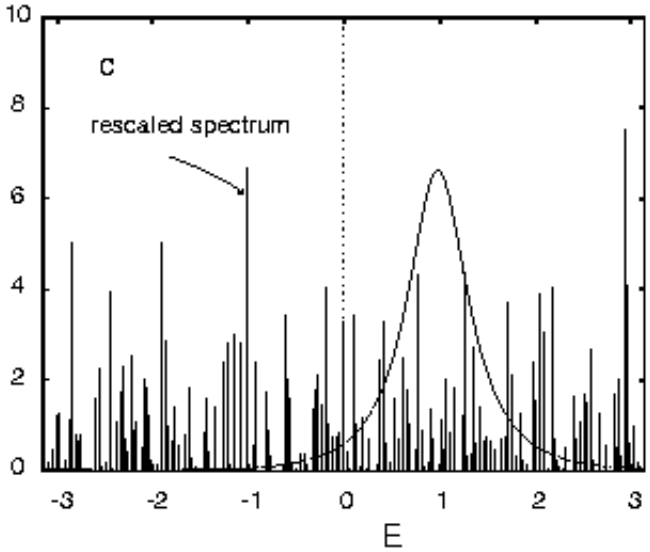
c
rescaled spectrum
E

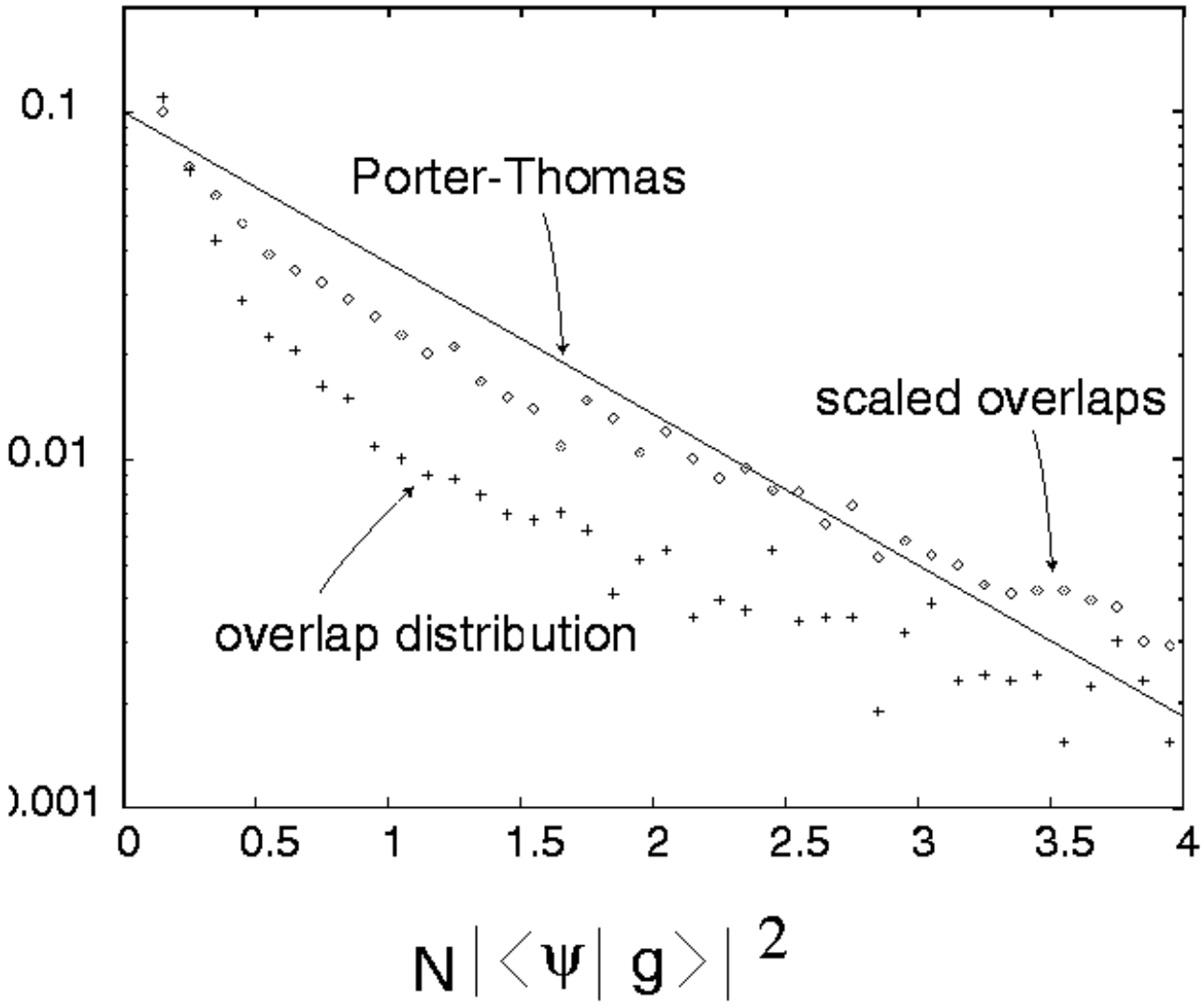
0.1
0.01
).001
0
0.5
1
1.5
2
2.5
3
3.5
4
Porter-Thomas
scaled overlaps
overlap distribution
N | ⟨ψ | g⟩ | 2

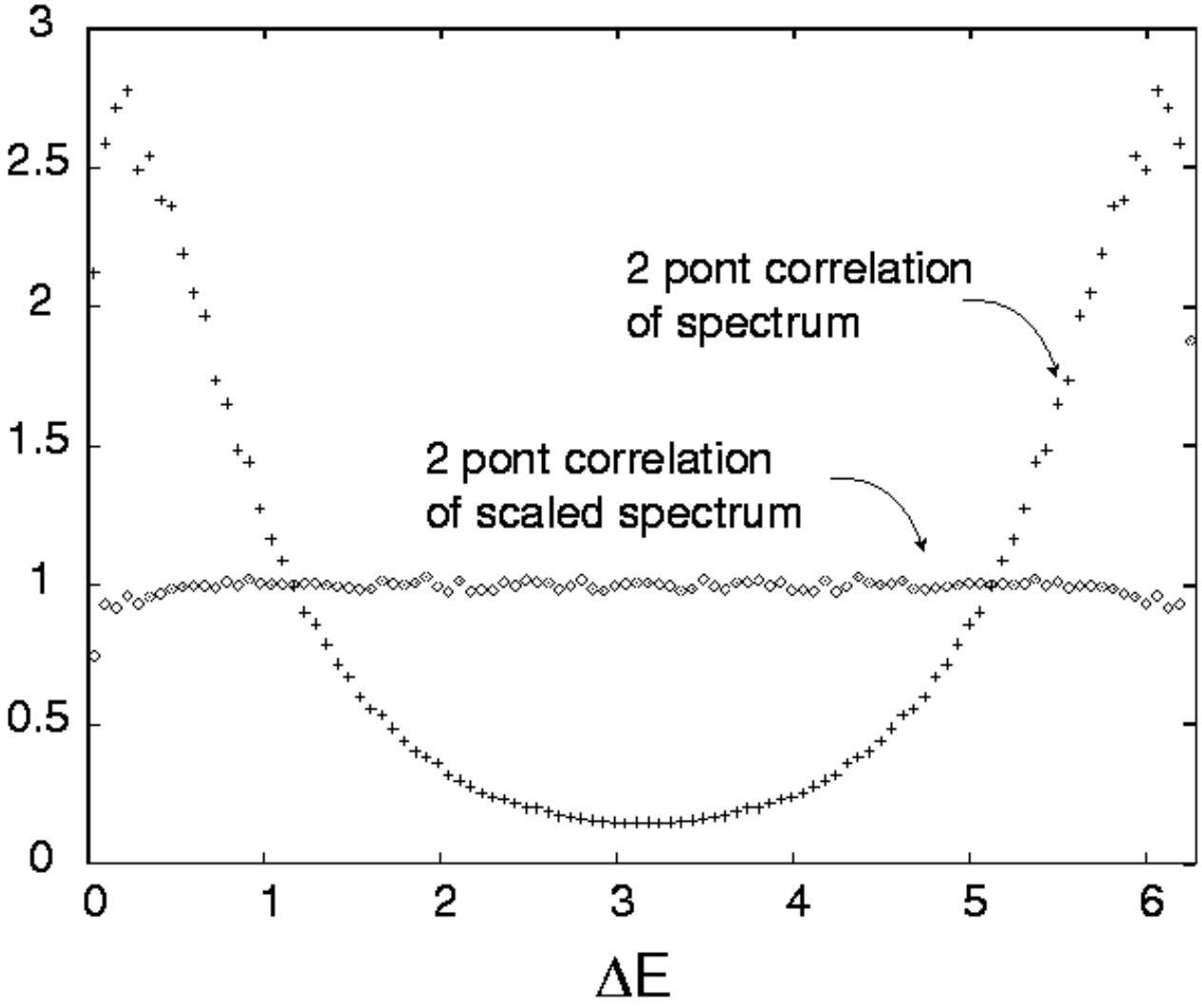
3
2.5
2
1.5
1
0.5
0
0
1
2
3
4
5
6
2 pont correlation
of spectrum
2 pont correlation
of scaled spectrum
ΔE

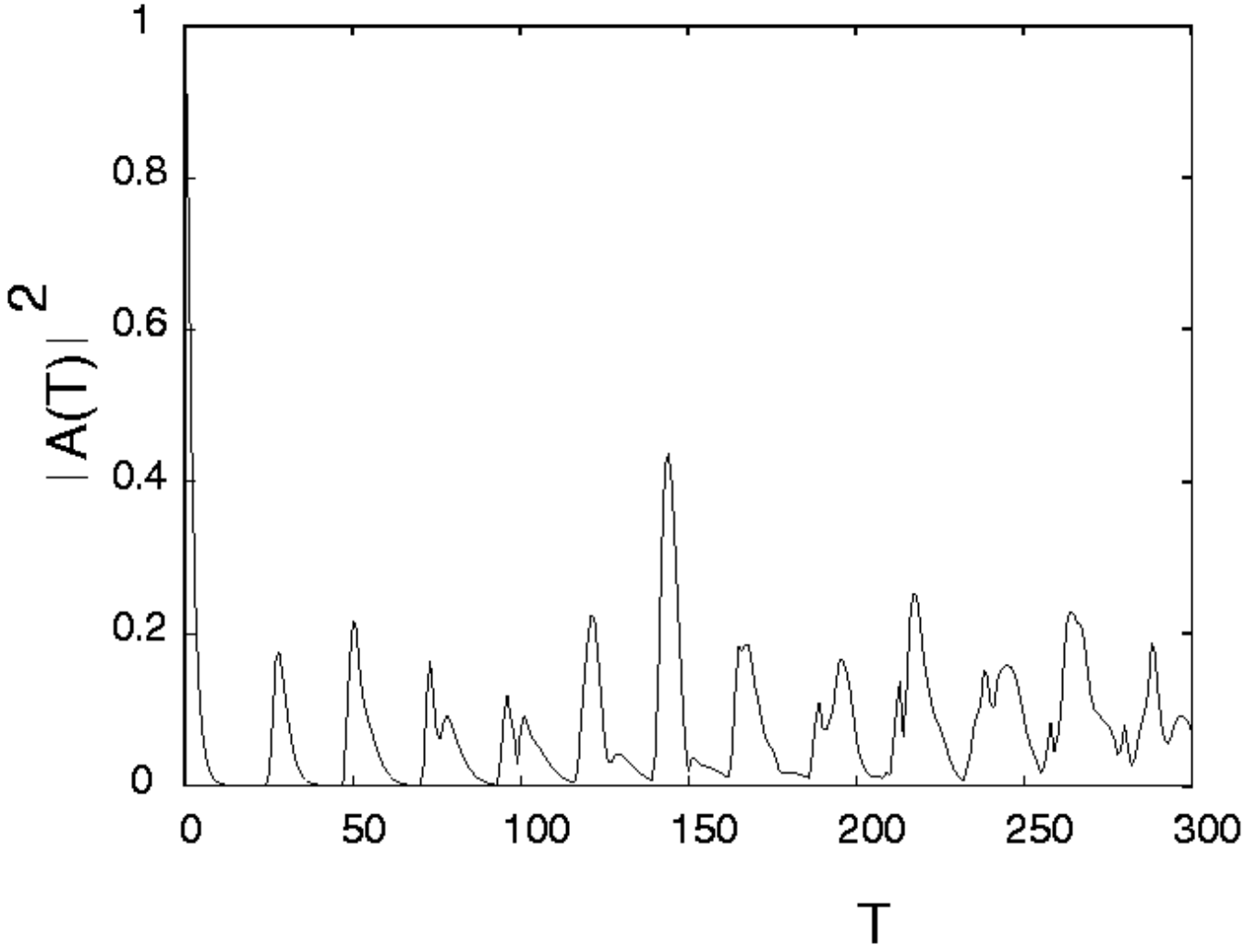
1
0.8
0.6
0.4
0.2
0
$|A(T)|^2$
0
50
100
150
200
250
300
T

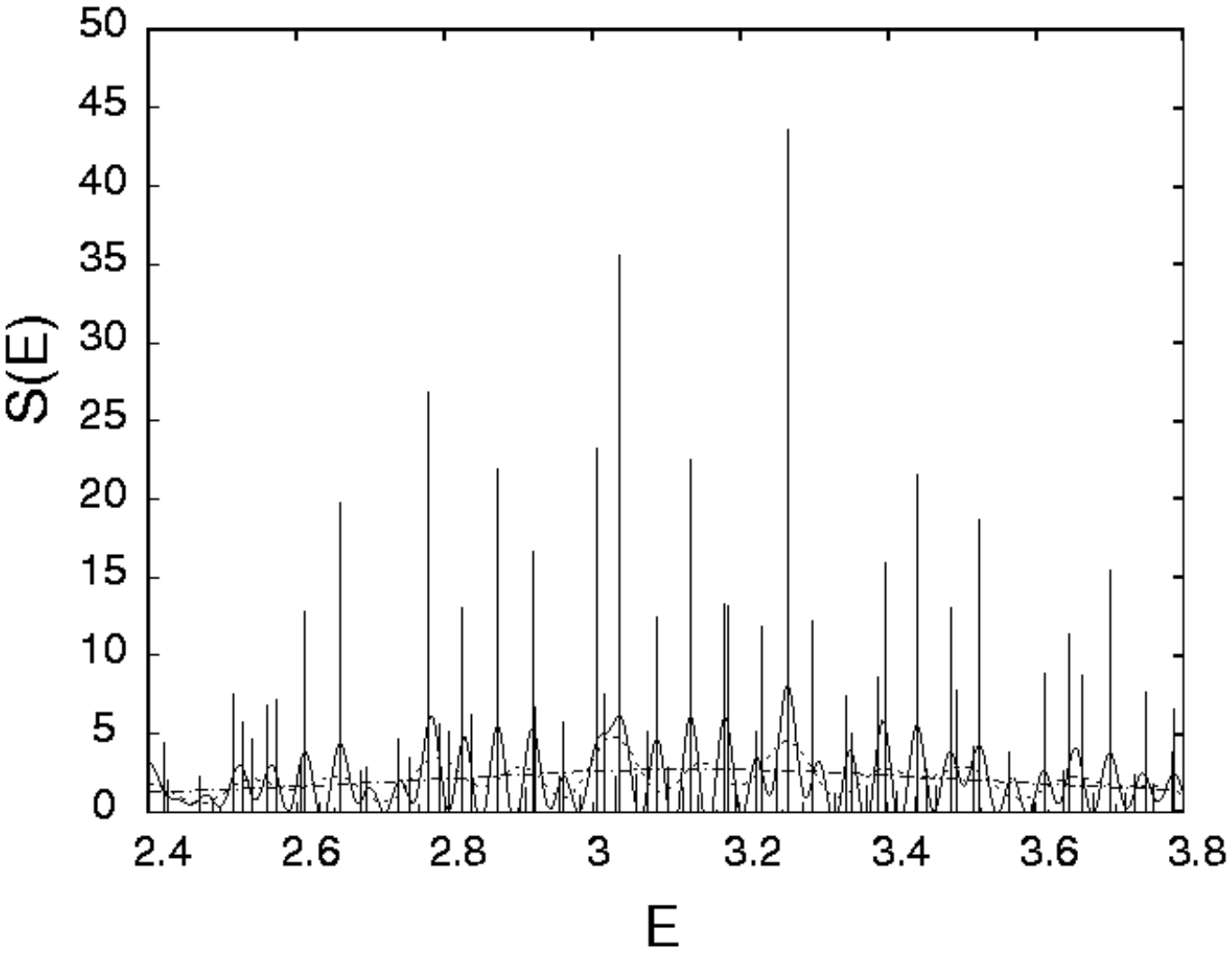
S(E)
E
50
45
40
35
30
25
20
15
10
5
0
2.4
2.6
2.8
3
3.2
3.4
3.6
3.8